Phase-Controlled Amplification of Few-Cycle Laser Pulses

Andrius Baltuška, Matthias Uiberacker, Eleftherios Goulielmakis, Reinhard Kienberger, Vladislav S. Yakovlev, Thomas Udem, Theodor W. Hänsch, and Ferenc Krausz

Invited Paper

***Abstract*—Intense ultrashort waveforms of light that can be produced with an exactly predetermined electromagnetic field are essential in a number of applications of extreme nonlinear optics, most prominently in laser-driven sources of high-energy attosecond radiation. Field reproducibility in each laser shot requires stabilization of the carrier-envelope phase. The authors analyze different schemes of phase-stable pulse amplification and identify constraints limiting the precision with which the phase can be maintained. Next, they describe a phase-stabilized laser system based on a 20-fs multipass Ti:sapphire amplifier supplemented with a fiber compression stage for producing pulses in the few-cycle regime. It is shown that the amplifier introduces only a slow millihertz phase drift and, therefore, can be seeded by a standard phase-stabilized oscillator. This residual phase drift is assigned primarily to the beam pointing instability and can be precompensated in the phase-control loop of the seed oscillator using a feedback signal from a phase detector placed in the amplifier output. The phase stability of the resultant 5-fs 400-μJ pulses at a 1-kHz repetition rate is subsequently independently verified by higher order harmonic generation, in which different carrier-envelope phase settings are shown, both theoretically and experimentally, to produce distinctly different spectral shapes of the XUV radiation. From a series of such spectral patterns, the authors succeed in calibrating the value of the carrier envelope phase (with a $\pm\pi$ ambiguity), which in turn allows them to fully characterize the temporal structure of the electric field of the laser pulses. The estimated precision of the phase control on the XUV target is better than $\pi/5$, which reduces the timing jitter between the driving laser pulse and the XUV bursts to $\sim$ 250 as and opens the way to generate stable isolated attosecond pulses.**

***Index Terms*—Frequency conversion, nonlinear optics, nonlinear wave propagation, optical pulse measurements, ultrafast optics.**

Manuscript received March 18, 2003; revised July 7, 2003. This work was supported in part by the FWF (Austria) under Grant P15382, Grant Z63, and Grant F016 and by the European Atto Network.

A. Baltuška, M. Uiberacker, E. Goulielmakis, R. Kienberger, and V. S. Yakovlev are with the Institut für Photonik, Technische Universität Wien, A-1040 Wien, Austria (e-mail: andrius.baltuska@tuwien.ac.at).

T. Udem and T. W. Hänsch are with the Max-Planck-Institut für Quantenoptik, D-85748 Garching, Germany.

F. Krausz is with the Institut für Photonik, Technische Universität Wien, A-1040 Wien, Austria. He is also with the Max-Planck-Institut für Quantenoptik, D-85748 Garching, Germany.

Digital Object Identifier 10.1109/JSTQE.2003.819107

I. Introduction

THE STEADILY expanding applications of ultrafast laser science demand an ever-increasing degree of control over many parameters of intense ultrashort laser pulses. Some forms of control, such as techniques of adjusting the spatial and temporal intensity pulse profiles as well as the sweep of the carrier frequency (chirp) across the electric field are already well established [1]. There are also well-developed methods for pulse diagnostics that can fully characterize the envelope of the pulse and its chirp [2], [3] and are an integral part of any control scheme. New demands, like control over the time-dependent polarization state of the pulse field on the scale of a single optical cycle [4], emerge in the context of strong field applications that are sensitive to the strength of individual light wave-cycles within the laser pulse rather than to its intensity envelope.

As advanced broad-band laser systems now approach the single-cycle regime [5]–[8], the electric field strength of the emitted pulses varies substantially from peak to peak of every optical half-cycle. Therefore, for such ultrashort waveforms of light employed in field-sensitive experiments, it becomes necessary to control precisely the evolution of the electric field underneath the pulse envelope. The parameter that determines the offset of the most prominent field peak with respect to the pulse envelope is the carrier-envelope (CE) phase. The change of the CE phase represents the slippage of the carrier wave through the pulse envelope, which has been shown to take place in conventional mode-locked laser systems [9], i.e., those without CE phase stabilization.

The proposal of techniques suitable for CE phase stabilization of mode-locked oscillators [10]–[12] and demonstration of such laser systems [13], [14] was a significant step toward accomplishing the full control over temporal as well as spectral properties of femtosecond laser pulses. Maintaining the value of the CE phase and the repetition frequency fixed also manifests itself in the frequency domain as a perfectly defined and steady comb of laser modes across the laser bandwidth and thereby provides an invaluable tool for frequency metrology [10], [11], [15]–[20]. Driven by the demand for simple, precise, and robust instrumentation for frequency measurements, the technology of CE phase control of mode-locked femtosecond lasers has rapidly matured [18], [19] and is now commercially available [21]. In comparison with laser oscillators operating at megahertz to gigahertz repetition rates, phase stabilization of laser amplifiers is

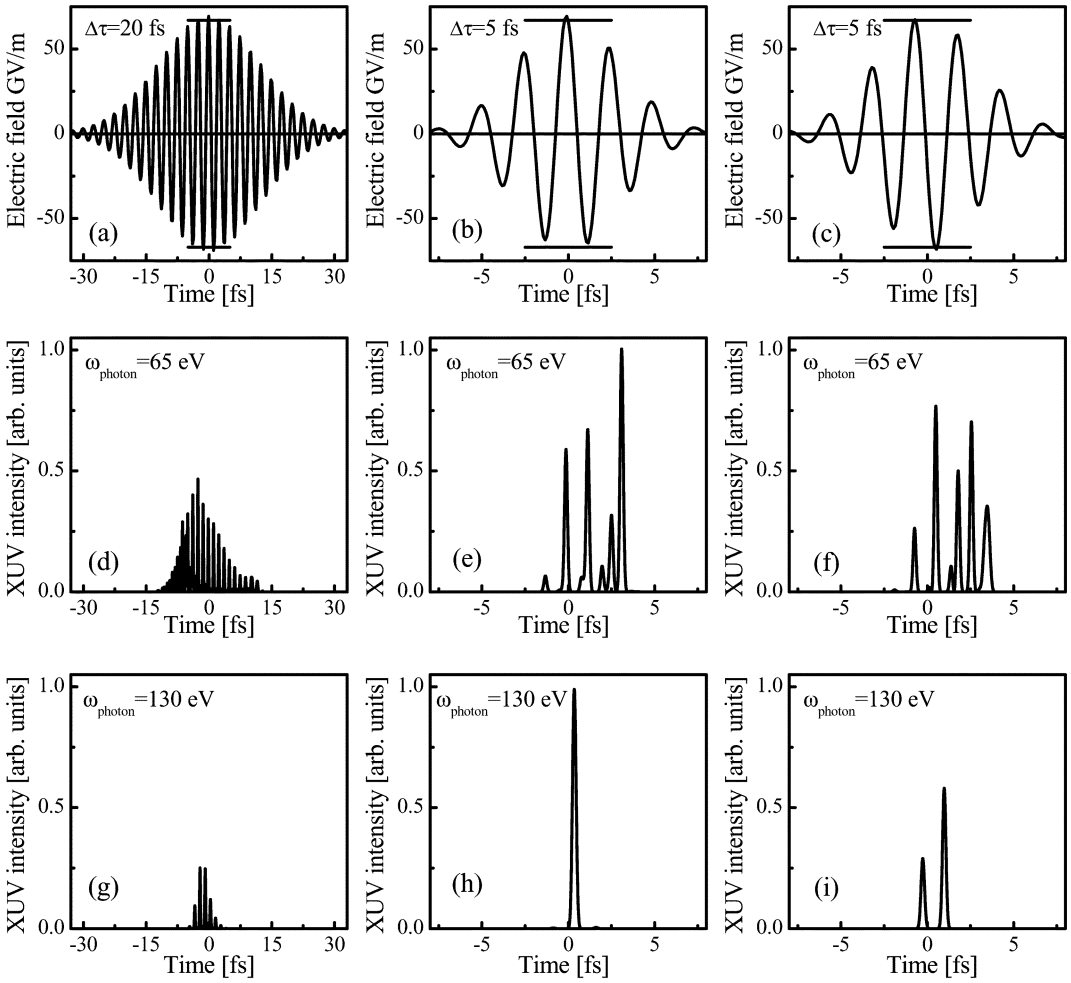

Fig. 1. Numerical simulation of laser-driven soft-X-ray emission from noble gas atoms. (a) Electric field of a 20-fs laser pulse. (b) Electric field of a 5-fs laser pulse optimized for generation of a single subfemtosecond X-ray pulse. (c) Electric field of a 5-fs pulse producing two highest energy X-ray pulses. (d)–(f) Time-domain structures of X-ray radiation emitted in a 10-eV bandwidth at half the cutoff energy. (g)–(i) Time-domain structures of X-ray radiation emitted in a 10-eV bandwidth at the cutoff energy. In this calculation, a neon gas target has the length of 2 mm and the pressure of 100 mbar. Pulse intensity was chosen to reach the cutoff frequency of 130 eV. Lower X-ray peak yield in (d) and (g) in comparison with (e), (f), (h), and (i) is the consequence of higher ionization by more numerous field peaks of the 20-fs pulse. In total, gas concentration loss due to ionization was 6.7% and 1.7% for the 20- and 5-fs pulses, respectively. Horizontal bars in (a)–(c) show peak intensity threshold required to yield cutoff-frequency X-ray radiation.

significantly complicated by their low, typically 1–10 kHz, repetition rate. Whereas it is possible to trace the CE phase offset in the output of an oscillator and compensate it by active stabilization of the laser cavity [13], [14], the output of a standard chirped pulse amplification system (CPA) is random [22]–[24]. Therefore, the information on phase excursions monitored behind the amplifier is insufficient for the phase stabilization of the kilohertz output pulse train, and other techniques, possibly in combination with the use of an already phase-stabilized seed oscillator, are required. Several different strategies toward CE stabilization of amplified laser pulses will be discussed in this paper.

The significance of the CE control of intense ultrashort laser pulses, as well as the motivation for pursuing it, can be readily grasped from the numerical example presented in Fig. 1. This simulation compares the XUV/ soft-X-ray emission from a target of noble gas exposed to three different driving optical fields depicted in Fig. 1(a)–(c). The generation scheme of the soft-X-ray radiation [25], [26] includes the following steps: ionization occurring in the vicinity of intense field peaks, acceleration of the detached electrons by the laser electric field, and recombination of the electron into its ground state following a recollision with the parent ion, whereupon the sum of the binding and the kinetic energy of the electron is released as a high-energy photon. Notably, the highest-energy soft-X-ray quanta, which are emitted at the so-called cutoff frequency, appear after approximately two-thirds of the optical cycle following the moment of ionization. This release of a photon nearly coincides with the first zero crossing of the electric field behind the strongest field peak.

Fig. 1(d)–(i) shows the corresponding temporal structure of the soft-X-ray radiation emitted around 65 and the 130 eV, respectively. The latter photon energy represents the cutoff obtainable under the chosen conditions that are listed in the caption of Fig. 1. It is obvious from Fig. 1(d) and (g) that for a 20-fs pulse, typical to many currently available laser amplifiers, the X-ray bursts are emitted repeatedly over many successive optical cycles. For this driving laser pulse the threshold of field strength [horizontal bars in Fig. 1(a)–(c)], required to generate cutoff frequency X-ray photons, can be overcome by multiple field peaks

because of their comparable magnitude. Consequently, regardless of the CE phase setting, the emitted X-ray will consist of a train of attosecond spikes.

The situation changes dramatically for a 5-fs driving pulse [Fig. 1(b) and (c)]. Whereas the emission at half the cutoff energy also comprises a train of spikes [Fig. 1(e)–(f)], the soft-X-rays at the cutoff frequency [Fig. 1(h) and (i)] are extremely sensitive to the arrangement of the optical cycles in the driving laser field. A $\pi/2$ change in the CE phase determines whether a single half-cycle or two field peaks fulfill the threshold requirement that in turn leads to the generation of an isolated subfemtosecond pulse [Fig. 1(h)] or a pair of similar bursts [Fig. 1(i)].

The case study presented in Fig. 1 underscores several compelling reasons for seeking CE phase control of amplified laser pulses in conjunction with the generation of subfemtosecond pulses [27], [28] and their use in the emerging field of attosecond metrology [29], [30] and spectroscopy [31]. First, pulse-to-pulse fluctuations of the CE phase lead to an unstable temporal profile of the soft-X-ray pulses, including duration variations and, for some phases, strong prepulses. Second, variable CE phase results in great intensity instability of the soft-X-ray bursts, thus severely limiting their utility. Third, the CE phase shift also causes a timing jitter between the soft-X-ray burst and the envelope peak of the driving laser field, which further reduces the temporal resolution of excite-probe experiments that use the laser and the soft-X-ray pulses, respectively, as excitation and probe [31] and vice versa.

The implications of CE phase variations on the higher order harmonic generation (extending into the XUV/soft-X-ray range) have been studied in a number of papers [6], [25], [26], [32]–[34]. The lack of CE control has been identified as a cause of an excessive spectral noise observed experimentally in X-ray spectra [35], [36]. Similar critical dependence on the value of the CE phase is expected in other nonlinear optical interactions that exhibit a threshold with respect to the field strength of the incident laser pulse [6]. In particular, the first clear experimental evidence of a CE phase-dependent effect was obtained in an above-threshold ionization measurement in gas [37]. In this scheme, the angular yield of photoelectron emission was found to be in correlation with the CE-phase of the circularly polarized driving pulses. Once CE phase-stabilized pulses at the required intensity level become available, it should be possible to steer photoelectrons from gas [37] or solid [38], [39] targets in a predefined way by adjusting the phase of light. In principle, CE phase control of laser pulses would open the way to synthesize intense waveforms of light, i.e., very brief high-peak-intensity electromagnetic fields exactly reproducible in every laser shot, which could be used to control the motion of charged particles with an ultimate precision.

Next to phase stabilization, an essential part of CE phase control is the measurement of the actual phase value. Standard techniques of pulse characterization [2], [3] are insensitive to CE phase since its value has no influence on the shape of the pulse envelope. Information on the relative pulse-to-pulse phase drift can be obtained by various methods involving interference of spectrally overlapping harmonic orders [11], [12], [14], [22], [24], [40], [41]. However, such techniques do not permit phase calibration either. Instead, the use of various high-order nonlinear responses has been suggested for this purpose [6], [33], [42], [43]. In the context of the numerical example, presented in Fig. 1, we have seen that phase calibration is needed to ascertain the presence of isolated attosecond pulses, especially if such pulses are intended for time-resolved attosecond applications.

This paper investigates both the problem of CE phase stabilization of amplified ultrashort laser pulses as well as a method of phase calibration that would be straightforward to implement in experiments utilizing the generation of subfemtosecond XUV pulses. Several possible schemes of CE phase control capable of operating at kilohertz repetition rates are addressed. We look into the origin of phase distortion added throughout pulse amplification and beam passage through peripheral components, such as dispersive pulse compressors and stages of nonlinear spectral broadening. We then explain in detail the operation of a CE phase-stabilized multipass Ti:sapphire 5-fs amplifier, which has been reported recently in a brief letter form [44]. Next, the attention is focused on the problem of measuring the actual value of the CE phase. To perform such phase calibration, we develop a method relying on spectral observation of XUV emission from a noble gas. The robustness of this approach is confirmed both experimentally and by numerical simulations. Subsequently, based on the parameters of the phase stabilization loop and the results of the independent experimental verification by XUV spectral measurements, we evaluate the CE phase stability presently available in our system.

II. CE Phase of a Mode-Locked Pulse Train and a Single Pulse

The temporal evolution of a linearly polarized electric field of a single pulse of light can be expressed in the following form:

$$E_L(t) = A_L(t)\cos\left[\omega_L(t)t + \varphi\right]. \tag{1}$$

This description includes three physical quantities: the amplitude $A_L(t)$, the frequency of field oscillations $\omega_L(t) = \omega_0 + \beta(t)$, and the CE phase φ. The latter parameter determines the timing of the carrier wave oscillations with respect to the amplitude envelope $A_L(t)$, whereas $\beta(t)$ stands for a possible chirp, i.e., a carrier frequency sweep across the pulse. The actual relationship between the carrier wave and the envelope changes as the result of pulse propagation through a dispersive medium. Therefore, (1) is only relevant to a specific coordinate. Also, referring to a CE phase-stabilized pulse train, we mean that at a given point in space every pulse has the same parameters in (1) and imply that the phase evolution with propagation is identical for all these pulses.

For applications of nonlinear optics that are sensitive to the strength of individual field peaks, a change in φ makes a physically measurable difference only if the amplitude is subject to significant variation within the light period $T_0 = 2\pi/\omega_0$, i.e., $|\partial A_L(t)/\partial t| \approxeq |2\pi/(T_0)AL(t)|$. Evidently, this condition is fulfilled in the case of 5-fs pulses [Fig. 1(b) and (c)], in which the XUV emission sensitively depends on φ, as opposed to the case of a 20-fs pulse [Fig. 1(a)], where the strength variation

between neighboring peaks is substantially smaller. Nevertheless, CE phase preserves a clear meaning regardless of the pulse duration. This can be easily understood by invoking the frequency-domain representation of a mode-locked laser spectrum [10]–[12], [16]–[19], [45]. The frequency of each individual laser mode ω_n can be expressed as

$$\omega_n = n\omega_{\mathrm{rep}} + \omega_{\mathrm{CE}} \tag{2}$$

where n is the mode number, ω_{rep} is the repetition rate of the laser, and ω_{CE} is a frequency shift from an exact integer multiple of ω_{rep}. Equation (2) describes the comb of frequencies across the mode-locked bandwidth that is of interest to applications of frequency-domain metrology [18]. The physical origin of the frequency mismatch ω_{CE} lies in the mismatch between the group delay (the cavity roundtrip time of the pulse envelope) and the phase delay (the roundtrip of the carrier wave). Consequently, the CE phase (i.e., the position of the carrier wave oscillation with respect to the envelope that is advancing at a different velocity) is shifted with each successive laser pulse by

$$\Delta\varphi = 2\pi\frac{\omega_{\mathrm{CE}}}{\omega_{\mathrm{rep}}}. \tag{3}$$

The phase slippage [9] $\Delta\varphi$ can be compensated by managing the cavity dispersion [13], [15], [15], [16], [40], [46], thereby forcing all emitted pulses to carry the same value of φ. It is interesting to notice that the reduction of the repetition rate, for example performed by selecting every mth pulse with a pulse picker in front of a CPA system, leads to an m-fold increase of the mode density but does not scale the frequency mode mismatch, which remains to be $\mathrm{mod}_{\omega_{\mathrm{rep}}/m}\{\omega_{\mathrm{CE}}\}$. In fact, the generation of new frequency modes is the result of applying a modulation that is nonlinear in the time domain (the fast switching of the pulse picker). This nonlinearity, however, does not destroy the properties of the frequency comb, as all the modes remain rigorously locked to each other. The same reasoning applies to the case of a single isolated laser pulse $\omega_{\mathrm{rep}} = 0$, which corresponds to a laser spectrum, $I_L(\omega)$, that is continuously filled with frequencies. In this treatment, φ can be interpreted as a frequency-independent offset of the spectral phase $\phi_L(\omega)$, which is immediately apparent from the following Fourier-transform link between the time- and frequency-domain electric field:

$$E_L(t) = \frac{1}{2\pi}\int \sqrt{I_L(\omega)}\exp\left[i\left(\phi_L(\omega) - \omega t + \varphi\right)\right]d\omega + c.c. \tag{4}$$

Here, the intensity spectrum $I_L(\omega)$ and the phase $\phi_L(\omega)$ fully determine the quantities $A_L(t)$ and $\omega_L(t)$ [2] but do not specify the carrier wave offset. The spectral manifestation of φ, given by (4), is particularly valuable describing various single-shot measurements of the CE phase offset throughout the paper.

III. Measurement of Phase Variations

In this section, we will address the practical methods for characterizing the changes in the CE phase, which are vital for implementing phase-stabilizing feedback loops that will be discussed subsequently.

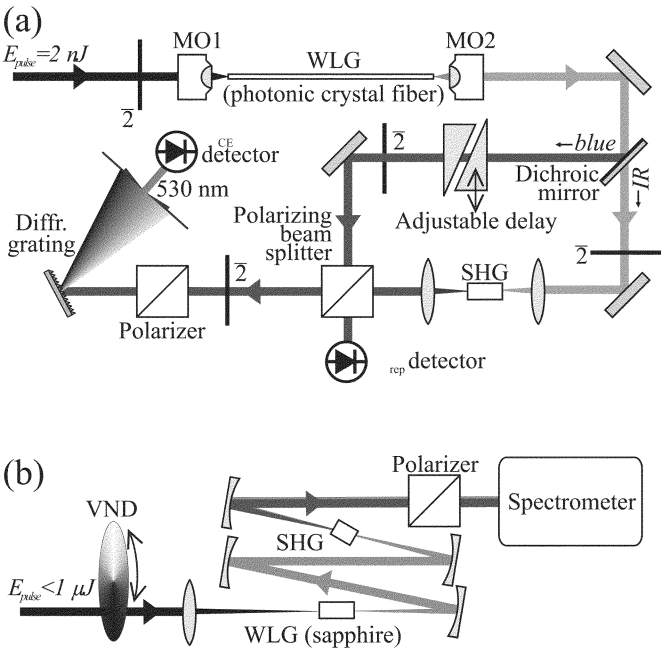

Fig. 2. Schemes for measurement of CE phase drift. (a) Nonlinear Mach-Zender interferometer for characterization of low-energy mode-locked oscillators. (b) Setup for phase characterization of amplified pulses by nonlinear spectral interferometry. MO1,2, microscope objective lenses. VND, variable neutral density filter. SHG, sum frequency generator. WLG, white light generator. $\lambda/2$, half-wavelength waveplates.

A. Detecting CE Drift of Oscillator Pulses

The standard tracking technique, employed in several CE phase-controlled oscillators [13], [14], [17]–[19] and later in this work, relies on detecting the frequency beat from the laser modes of the frequency comb which are separated by a spectral octave, i.e., differ in their frequency by a harmonic order. The lower frequency mode is then frequency doubled and the two modes are brought in interference with each other producing a beat at the CE frequency

$$\omega_{\mathrm{CE}} = 2\left(n\omega_{\mathrm{rep}} + \omega_{\mathrm{CE}}\right) - \left(2n\omega_{\mathrm{rep}} + \omega_{\mathrm{CE}}\right). \tag{5}$$

This scheme requires the presence of a very broad-band octave-spanning spectrum that is unavailable from a typical mode-locked oscillator. To gain the necessary bandwidth, the laser spectrum can be broadened by white-light generation (WLG) in a medium with a third-order nonlinearity. Using a photonic crystal fiber (PCF) [47]–[49], this task can be accomplished even with nanojoule pulses from an oscillator. The device incorporating the spectral broadening, frequency doubling, generating the beat signal is called nonlinear interferometer or, for short, f-to-$2f$ setup. In state-of-the art broad-band mode-locked oscillators, it has already become possible to derive the f and the $2f$ frequency components directly from the laser spectrum, thus obviating the need for extracavity spectral broadening [50], [51].

Fig. 2(a) presents the schematic of a generic f-to-$2f$ unit. The beam is coupled into a piece of PCF, and recollimated behind it with a pair of microscope objective lenses. The blue-shifted part of the resultant white light is separated from the red-shifted spectral wing with a dichroic mirror. A fraction of the infrared beam is then frequency doubled in the second-harmonic generation crystal (SHG) [Fig. 2(a)] and recombined with the blue por-

tion of the white light continuum on a polarizing beamsplitter. Two glass wedges in one of the interferometer arms are used to adjust the timing of the two interfering wave packets. The polarizing cube enables their interference by selecting a common polarization component of the beams. Several half-wave plates are employed for choosing polarizations appropriate for the frequency doubling and the subsequent interference. A bandpass filter, consisting of a diffraction grating and a slit, selects a narrow frequency interval within the spectral overlap between the white light and its frequency-doubled part. This filtering enables observation of a beat between two quasi-monochromatic frequency components, as suggested in (5). Two avalanche photodiodes detect the repetition frequency $\omega_{\rm rep}$ and the offset frequency $\omega_{\rm CE}$, respectively. According to (3), the information provided by the measurement of $\omega_{\rm rep}$ and $\omega_{\rm CE}$ is sufficient to characterize the drift of CE phase. The use of these inputs will be addressed below in the description of the feedback loop for CE phase stabilization of an oscillator.

B. Detecting CE Drift of Amplified Pulses

We now turn our attention to the phase drift characterization of amplified laser pulses. Compared with the case of an oscillator, there are three significant differences. First, the repetition rate of the amplifier must be lowered, typically by five orders of magnitude, to 1–10 kHz, which complicates accurate detection of $\omega_{\rm rep}$ and $\omega_{\rm CE}$. Second, the availability of high-energy pulses simplifies the problem of producing an octave-spanning white-light continuum. Third, laser amplifiers exhibit a considerably higher peak intensity noise compared with "quiet" Kerr-lens-mode-locked oscillators [52]. Consequently, the excursions of a quasi-monochromatic f-to-$2f$ signal detected behind the amplifier do not necessarily suggest a change of the CE phase but might reflect pulse energy fluctuations.

Amplifier phase tracking schemes reported to date [22], [24], [44] took advantage of the abundant pulse energy and utilized different types of single-shot nonlinear spectral interferometry. The objective of the method is to use broad-band detection of the f-to-$2f$ beat as opposed to the narrow-band scheme acceptable in the case of an oscillator. Briefly, the essence of this approach can be described as follows. After generating a sufficiently broad-band white-light spectrum, $I_{\rm WL}(\omega)$, the pulse is sent to an SHG crystal resulting in a field up-shifted with frequency

$$\begin{aligned} E_{\rm SHG}(\omega) \propto & \exp(i2\varphi) \int \chi^{\langle 2\rangle}(\omega:\omega',\omega-\omega') \\ & \times \sqrt{I_{\rm WL}(\omega')I_{\rm WL}(\omega-\omega')} \\ & \times \exp\left[i\left(\phi_{\rm WL}(\omega')+\phi_{\rm WL}(\omega-\omega')\right)\right] d\omega' \\ = & \sqrt{I_{\rm SHG}(\omega)}\exp\left[i\left(\phi_{\rm SHG}(\omega)+2\varphi\right)\right] \end{aligned} \tag{6}$$

where $\phi_{\rm WL}(\omega)$ is the spectral phase of the white light and $\chi^{\langle 2\rangle}$ is the second-order susceptibility. The interference between the white light and SHG pulses, separated by the time delay τ_0, can be then written as follows:

$$\begin{aligned} S(\omega) = & (1-a)I_{\rm WL}(\omega) + aI_{\rm SHG}(\omega) \\ & + 2\sqrt{a(1-a)I_{\rm WL}(\omega)I_{\rm SHG}(\omega)} \\ & \times \cos\left(\phi_{\rm SHG}(\omega)-\phi_{\rm WL}(\omega)+\omega\tau_0+\varphi\right) \end{aligned} \tag{7}$$

where the coefficient a stands for the polarizer transmission for the polarization of the SHG light. For a sufficiently large pulse separation τ_0, which corresponds to many spectral fringes in the interferogram $S(\omega)$, the argument of the cosine in (7) can be recovered using the standard algorithm of Fourier transform spectral interferometry (FTSI) [53]. This procedure consists of Fourier transforming into the time domain, applying a bandpass filter around $t=\tau_0$ (or, alternatively, around $\tau=-\tau_0$), and another Fourier transformation back to the frequency domain. The phase of the newly obtained complex spectral function then directly yields the differential phase of the two fields, $\mathrm{mod}_{2\pi}\{\phi_{\rm SHG}(\omega)-\phi_{\rm WL}(\omega)+\varphi\}$. In principle, such interference measurement can be used not only to characterize the pulse-to-pulse changes of φ, but even to find the actual value of φ. In practice, however, this is not feasible because with the currently available methods, $\phi_{\rm SHG}(\omega)$ and $\phi_{\rm WL}(\omega)$ can only be characterized with the precision of an arbitrary constant [2]. Only by fully accounting for the evolution of the spectral phase in the SHG crystal, which includes both linear and nonlinear pulse propagation, would it be possible to retrieve the value of φ in this scheme. Therefore, the f-to-$2f$ interferometer can only measure the full CE phase after calibration by an independent external experiment, as will be shown in Section VII. Otherwise, this device reflects the phase jump in the jth laser pulse with respect to another (e.g., 0th) pulse arriving earlier from the same pulse train and chosen as reference, i.e., the interferometer measures $\delta\varphi_j=\varphi_j-\varphi_0$.

The difference between the method outlined above and the FTSI based on the use of parametric waves, reported in [24], is that in the latter case one measures the interference between the frequency-doubled idler and the signal pulses. The advantage in this case is that the white-light continuum, injected into the parametric device, does not have to span an octave and that the interference is observed close to the spectral peak of the signal rather than in the continuum wing. In this work, however, we opted for a simpler setup, shown in Fig. 2(b), similar to the scheme published in [22]. For further simplification, we have replaced the WLG in a hollow waveguide with bulk continuum generation in a 2-mm sapphire window. Because of the dispersion of this window and of the 1-mm BBO frequency-doubling crystal, the white light and SHG are sufficiently separated in time to employ the FTSI routine described above. The spectral interferogram is measured by a fiber-coupled spectrometer (S2000, Ocean OMA) behind a polarizer cube that selects the common polarization of the beams. With a 2-MHz acquisition card (AD2000, Ocean Optics) single-shot f-to-$2f$ interferograms can be detected for every third laser shot at a 1-kHz repetition rate.

The two types of f-to-$2f$ interferometers, presented in Sections III-A and B, possess many common traits but have also a difference in their sensitivity to mechanical vibrations. In the device shown in Fig. 2(a), the variation of the interferometer arm length affects the strength of the signal at the beat frequency $\omega_{\rm CE}$, but does not directly influence the precision of the measurement of $\omega_{\rm CE}$. In fact, the sensitivity to timing reflects the fact that we are dealing with quasi-monochromatic wave packets selected from the white light and its SHG pulse rather than with purely monochromatic frequency modes. In the f-to-$2f$ unit shown in Fig. 2(b), the timing jitter, $\tau=\tau_0+\delta\tau$, has an immediate impact on the fringe pattern of the measured

intefrerogram, as will be shown in Section III-C. However, for the collinear arrangement, depicted in Fig. 2(b), the problem of time jitter is negligible as the interfering beams follow the same path.

C. Measuring the Phase Difference by Linear Interferometry

Above, we have presented interferometric methods that employ (nonlinear) frequency conversion and reveal variations in the value of CE phase. Here, we will discuss the technique of linear spectral interferometry [54]–[56], which measures the phase difference between the test and reference arms of an interferometer. It is instructive to compare the relevance of this method to the characterization of CE phase drift with the situation in the measurement of pulse envelope and chirp. Indeed, if the intensity spectrum $I_L(\omega)$ and the phase $\phi_L(\omega)$ (with the precision of a *const*) are determined in front of an interferometer, and the phase accumulated inside the interferometer, $\phi(\omega)$, is recovered by FTSI, then the phase of the outgoing pulse is also known and equals $\phi_L(\omega)+\phi(\omega)$. Therefore, once $\phi_L(\omega)$ was found with a nonlinear optical technique (e.g., autocorrelation or frequency-resolved optical gating [2]), further complete phase characterization can be performed with linear methods, provided a reference beam derived after the nonlinear measurement is available. In essence, we have just stated the principle of the pulse measurement by temporal analysis by dispersing a pair of light E-fields (TADPOLE) [2].

Linear FTSI can be used exactly the same way to study CE phase deviations occurring behind a nonlinear f-to-$2f$ interferometer. To do so, a small fraction of the beam (reference) can be split behind the point where the changes of are tracked with the f-to-$2f$ unit and sent to propagate through free space (air). For practical purposes, fluctuations of air density are the only cause of CE phase jitter of the reference pulses, and, therefore, we consider these pulses CE phase stable. The main (test) beam is directed into an optical arrangement (e.g., an amplifier) and accumulates a phase difference $\phi(\omega)$ with respect to the reference. As the consequence of beam pointing instability during the propagation through elements with angular dispersion, and other linear and/or nonlinear dispersion changes [45], the test pulse can also pick up a frequency-dependent phase offset

$$\delta(\omega)=\delta(\omega_0)+\frac{1}{2}\delta'(\omega_0)(\omega-\omega_0)+\frac{1}{6}\delta''(\omega_0)(\omega-\omega_0)^2+\cdots. \quad (8)$$

We assume that $\delta(\omega)$ corresponds to a very minute dispersion modification that does not involve reshaping of the pulse envelope. Otherwise, if case $A_L(t)$ is modified, CE phase control would become irrelevant. Indeed, a tiny ($<1\,\mu$m) change in the propagation length within dispersive material already leads to a sizable leap in the CE phase [9], which we term $\delta\varphi$. Consequently, it is justified to disregard higher order terms, starting with the parabolic phase distortion. In fact, $\delta\varphi$ represents the sum of frequency-independent terms in (8). Next in significance is the linear with-frequency part of (8), which simply represents the time shift due to a modified propagation length and, therefore, has no bearing on the CE dynamics. Therefore, in the characterization of the phase drift of the test pulse, we will only pay attention to the phase jump $\delta\varphi$ and treat the test-reference timing offset separately.

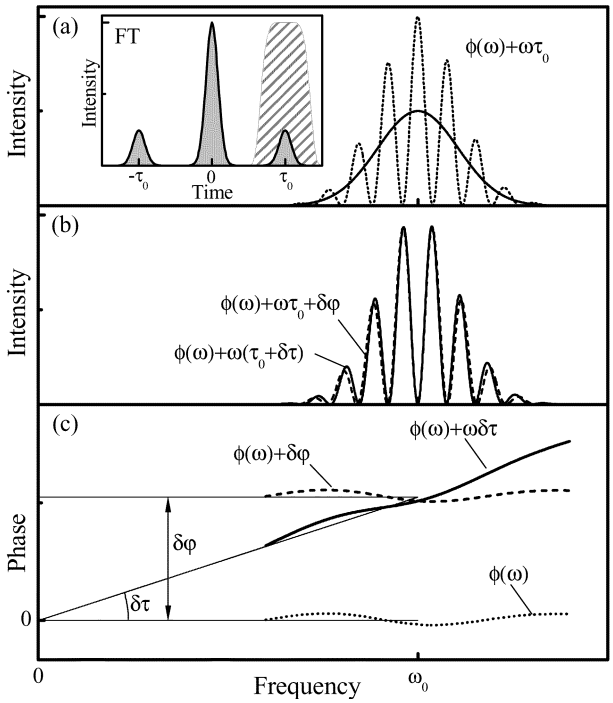

Fig. 3. Discrimination between phase and timing jitter in the Fourier-transform spectral interferometry. (a) Intensity spectrum (solid curve) and spectral interferogram (dotted curve). (b) Spectral interferograms modified by a timing shift (solid curve) and a frequency-independent phase shift (dashed curve). Note fringe period change in the case of timing shift. (c) Differential spectral phases after time-delay slope subtraction. Dotted and solid and dashed curves correspond to interferograms in (a) and (b), respectively. Inset shows the power spectrum of the Fourier transform to the time domain. Dashed contour corresponds to a possible filter required in the phase extraction to isolate the temporal peak at τ_0.

As has been pointed out in Section III-B, a temporal jitter between the interfering pulses causes fringe rearrangement in the spectrogram $S(\omega)$. This timing variation is inevitable, especially if the reference beam is not interferometrically stabilized. For large laser systems, the path of the reference beam can be several meters long and fluctuate within several light wavelength cycles. For that reason, the ability of FTSI (both linear and nonlinear) to discriminate between $\delta\varphi$ and the timing jitter needs to be scrutinized.

Fig. 3 gives an overview of FTSI properties. Fig. 3(a) shows a typical interferogram and the power spectrum of its Fourier transform (inset) used in phase retrieval. In Fig. 3(b), we examine the impact on the interferogram by a pure time shift $(\delta\tau)$ and a pure phase jump $(\delta\varphi)$, depicted by the solid and the dashed curves, respectively. The corresponding phases after subtracting the phase slope $\omega\tau_0$, which is due to the delay between the test and reference pulses, are presented in Fig. 3(c). The particular shape of the intensity spectrum $I_L(\omega)$ [solid curve in Fig. 3(a)] and differential phase $\phi(\omega)$ [dotted curve in Fig. 3(c)] are selected arbitrarily. The values of $\delta\tau$ and $\delta\varphi$ are chosen such that the interferograms in Fig. 3(b) closely resemble each other. Nevertheless, there is a fundamental difference due to the fact that the timing variation changes the fringe period, which can be clearly observed in an interferogram consisting of a large

amount of fringes. Therefore, using a charge-coupled device (CCD)-based spectrograph that covers the entire relevant spectral width and has a sufficiently high resolution, it becomes possible to separate the contributions of $\delta\varphi$ and $\delta\tau$ as long as FTSI noise criteria [55], [56] are met. Numerically, we have implemented the time jitter correction in our FTSI code by extracting a linear phase on the phase obtained by back-transformation into the frequency domain.

The immediate implication of the solution of the timing problem is the ability to trace CE phase jumps with respect to a reference beam propagating in free space. We believe this method can be particularly useful for extending CE phase stabilization in a multistage laser system, in which the earliest stage is phase-stabilized and the subsequent ones are expected to introduce slow phase drift only.

Summarizing this section, we have presented two types of nonlinear f-to-$2f$ interferometers for CE phase drift characterization of low-energy (several nanojoules) megahertz–gigahertz-repetition-rate oscillators and high-energy (starting from 1 μJ) kilohertz-repetition-rate amplifiers. We have also shown a linear phase drift detection that is complementary to the nonlinear techniques. Information on CE phase deviations, obtained with these methods, can be used as feedback for phase stabilization loops discussed in Section V.

IV. Phase Jitter of the White-Light Continuum

The f-to-$2f$ phase characterization methods presented in Section III, and indeed all phase-stabilized laser systems reported to date [13], [14], [19], critically rely on white-light continuum generation as means of creating a phase-coherent spectrally broadened replica of the input laser pulse. The phase noise added in the process of white light generation is an intrinsic problem of CE phase stabilization loops [19]. In this section, we first outline the reason for the phase coherence between the white light and the initial pulse and then study the influence of intensity fluctuations on the phase noise.

A. Phase Lock Between the Input Pulse and the White-Light Continuum

Generally, white-light generation consists of several nonlinear wave-mixing processes that lead to generation of new frequency components. Therefore, it is not immediately clear whether WLG can be relied on for producing a frequency-broadened but phase-offset-repeating replica of the laser pulse. The complete propagation equation for pulse self-action (assuming the perturbative regime of nonlinear optics [6]) can be derived directly from Maxwell's equation [6], [57]–[59] and written in the frequency domain as

$$\left[\nabla^2 + k^2(\omega)\right] E(\mathbf{r},\omega) = \frac{\omega^2}{\varepsilon_0 c^2} P^{nl}(\mathbf{r},\omega) \tag{9}$$

where $E(\mathbf{r},\omega)$ and $P^{nl}(\mathbf{r},\omega)$ denote the electric field and generated nonlinear polarization, respectively. The particular form of $P^{nl}(\mathbf{r},\omega)$, which describes both the delayed Raman response (i.e., slow nonlinearity) and the parametric four-wave mixing based on fast electronic Kerr nonlinearity, also known as the process of self-phase-modulation (SPM) [57]–[59], can be given by

$$\begin{aligned} P^{nl}(\mathbf{r},\omega) = &\iint \chi^{\langle 3\rangle}(\omega:\omega_1,\omega_2,\omega_1+\omega_2-\omega)E(\mathbf{r},\omega_1) \\ &\times E(\mathbf{r},\omega_2)E^*(\mathbf{r},\omega_1+\omega_2-\omega)d\omega_1 d\omega_2 \\ =&\exp\left[i\left(\varphi+\varphi-\varphi\right)\right] \\ &\times \iint \chi^{\langle 3\rangle}(\omega:\omega_1,\omega_2,\omega_1+\omega_2-\omega) \\ &\times \sqrt{I(\mathbf{r},\omega_1)I(\mathbf{r},\omega_2)I(\mathbf{r},\omega_1+\omega_2-\omega)} \\ &\times \exp\left[i\left(\phi(\mathbf{r},\omega_1)+\phi(\mathbf{r},\omega_2)-\phi(\mathbf{r},\omega_1\right.\right. \\ &\left.\left.+\ \omega_2-\omega)\right)\right] d\omega_1 d\omega_2 \end{aligned} \tag{10}$$

where $\chi^{\langle 3\rangle}$ represents the effective third-order susceptibility and the conjugation symbol marks emission [60]. The propagation-dependent change of dispersion is included in $\phi(\mathbf{r},\omega)$. Here, we assume that all mixing frequencies are positive [61]. The appearance of the conjugation operator in the convolution integral in (10) accounts for the preservation of the initial phase offset φ in the output field. After solving (9) over the interaction length of the WLG medium $\mathbf{r}_1 - \mathbf{r}_0$, the resultant output pulse will generally carry a different value of the CE phase [6], [62] than the input pulse (i.e., $\varphi_{\mathrm{WL}} \neq \varphi$), which is also the case for any type of dispersive linear or nonlinear pulse propagation. Nevertheless, the important moment for an accurate CE phase drift determination is the ability of the white-light continuum to repeat without distortion the input phase offset, which is the consequence of the rule for phase summation in (10). After plugging (10) in (9), φ cancels out, i.e., it has no effect on $\phi(\mathbf{r}_1,\omega)$ of the output field regardless of the microscopic origin of the nonlinearity. The presence of a resonant or nonresonant fifth-order parametric wave mixing (EE^*EE^*E) [63] does not lead to a φ-dependent propagation either. However, the solution for pulse propagation does become φ-dependent if SHG and/or third-harmonic generation (THG) cannot be neglected. To account for these contributions, $P^{nl}(\mathbf{r},\omega)$ should also include the terms describing the three-wave mixing of SHG and the four-wave mixing of THG, with their phase summation rules given by the field products EE and EEE, respectively.

Summarizing the considerations presented above, we would like to underscore two points. First, the phase shift added by both the nonresonant and/or resonant white-light generation does not depend on the CE phase of the input pulse. Therefore, these techniques of spectral broadening can be readily applied in the schemes measuring the CE phase drift. Second, the mixing in of undesired mechanisms of frequency conversion, such as SHG (or, in a broader sense,—sum frequency generation) and THG, can distort the frequency-independent phase of the white-light pulse even if there are no intensity fluctuations of the input pulse at all. In typical experimental conditions, however, SHG and THG do not play a significant role. For instance, nonphase-matched second harmonic radiation is often observed in the cladding of conventional single-mode fibers but it is probably not sufficiently strong to cause a noticeable pulse-to-pulse phase jitter. For bulk-material chirping (typically performed in sapphire or $\mathrm{CaF_2}$), the contributions of SHG and THG are negligible.

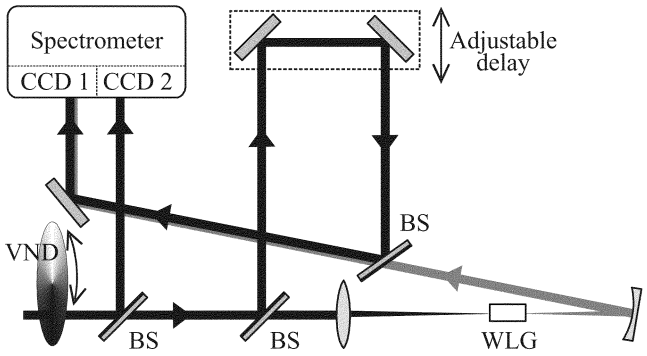

Fig. 4. Single-shot spectral interferometer for measurement of CE phase jitter arising from white light generation. VND, variable neutral density filter. BS, dielectric beamsplitter.

B. Phase Noise Resulting From Intensity Fluctuations

In Section IV-A, we have dismissed the interplay between different types of nonlinearity as a concern for added phase jitter in WLG. In practice, a much more important phase distortion is the variation of the intensity-induced phase shift [64]. As the result of intensity-dependent nonlinear interaction, the phase accumulated throughout the WLG can vary from pulse to pulse and compromise the fidelity of CE phase drift characterization. In the case of f-to-$2f$ interferometers suited for oscillators, these problems can arise from mechanical vibrations of the PCF, which affect the amount of light coupled in. In contrast, f-to-$2f$ interferometers for amplified pulses can employ bulk WLG (cf. Section III-B), which is almost insensitive to beam pointing fluctuations. Typical studies of WLG phase stability consist of interference measurements of independently produced white-light continua [65]–[67]. The influence of the WLG phase noise on the operation of phase-stabilization loops has also been investigated by measuring the CE drift with two independent PCF-based f-to-$2f$ interferometers [19], [68], [69].

Here, we check the phase jitter of the WLG in bulk sapphire, used in the f-to-$2f$ interferometer described in Section III-B, against increased intensity noise of amplified pulses [52]. The WLG stage of the unit shown in Fig. 2(b) was supplemented by a linear interferometer depicted in Fig. 4, which has allowed us to measure the phase shift of the white light with respect to the replica of the injected pulse. The intensity of the beam was being varied with a neutral density filter (VND in Fig. 4) while single-shot laser—white-light interferograms and laser spectra were being recorded by a dual-channel spectrometer. The synchronous registration of the laser spectra is necessary to calibrate the pulse energy in each laser shot.

We used a multipass Ti:sapphire amplifier, the CE phase-stabilization of which will be described in Section VI, with a root mean square (rms) intensity noise of 1%. The optimized setting of the neutral density filter corresponds to the pulse energy of 0.7 μJ in front of the sapphire window and the diameter of the focal spot of about 30 μm. These parameters allow us to generate the white-light bandwidth adequate for the f-to-$2f$ measurement. For these conditions, the rms phase jitter retrieved from the measurement of the laser—white-light interferogram is $\sim$100 mrad.

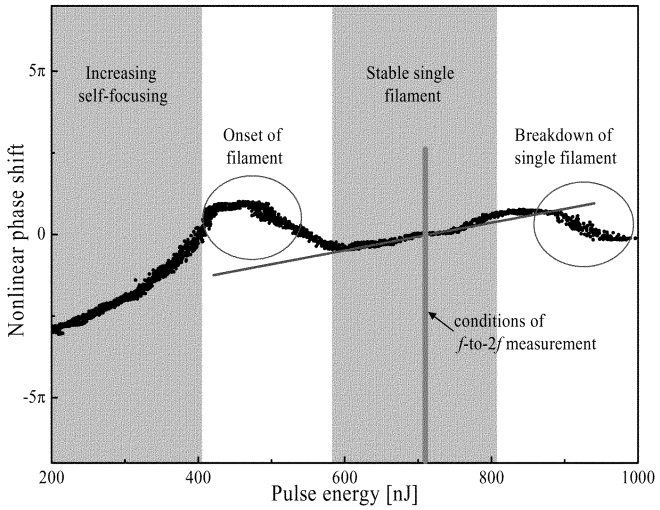

Fig. 5. Intensity-phase coupling of the white-light generation in bulk sapphire. Solid dots depict phase changes extracted from single-shot interferograms. Straight line shows a linear fit marking the slope of phase intensity-dependent variation in the vicinity of the pulse energy used for f-to-$2f$ characterization.

Next, we recorded phase statistics for various settings of the neutral density filter. The resultant phase evolution, plotted as a function of incident pulse energy, is presented in Fig. 5. The data cover several distinct regimes indicated in Fig. 5 by vertical sections. First, we notice that there is an abrupt phase change that corresponds to the increasing strength of self-focusing and filament formation. This can be explained by the change in the group velocity of light with the increase of the intensity-dependent part of the refractive index of sapphire. After the markedly noisy region of the onset of filamentation, the phase shows a certain "rebound" that probably indicates the increase of the filament length. This is followed by the interval of stable filamentation, which is relatively broad in terms of pulse energy—about $\pm$8% around the energy set point of the f-to-$2f$ setup. At higher pulse energies, we observe a collapse of the filament and multiple filamentation. The phase noise and the downward phase trend somewhat resemble the situation before the formation of a single stable filament. Measurement at even higher energies could not be performed with a multifilament beam because of the breakdown of the interference pattern into several modes.

In the regime of a stable filament, the phase exhibits a quasi-linear change with energy. The rate of this variation, given by the straight line in Fig. 5, is 12 mrad/nJ, which corresponds to a 84 mrad phase shift for a 1% jump in the pulse energy.

The presented phase evolution covers only the spectral overlap region between the white light and the input pulse, i.e., approximately a 60-nm bandwidth. Therefore, the results of our measurement correspond to the best-case scenario since phase excursions in the blue $(2f)$ spectral region cannot be visualized. Additionally, the SHG of the red-shifted part of the continuum also causes an intensity-dependent phase shift and, consequently, is likely to worsen the precision of the f-to-$2f$ CE phase drift characterization further.

The considerations about the phase properties of WLG, presented in this section, are important to identify the limitations of CE phase control schemes discussed below and to evaluate the applicability of WLG as a tool for extending a mode-locked

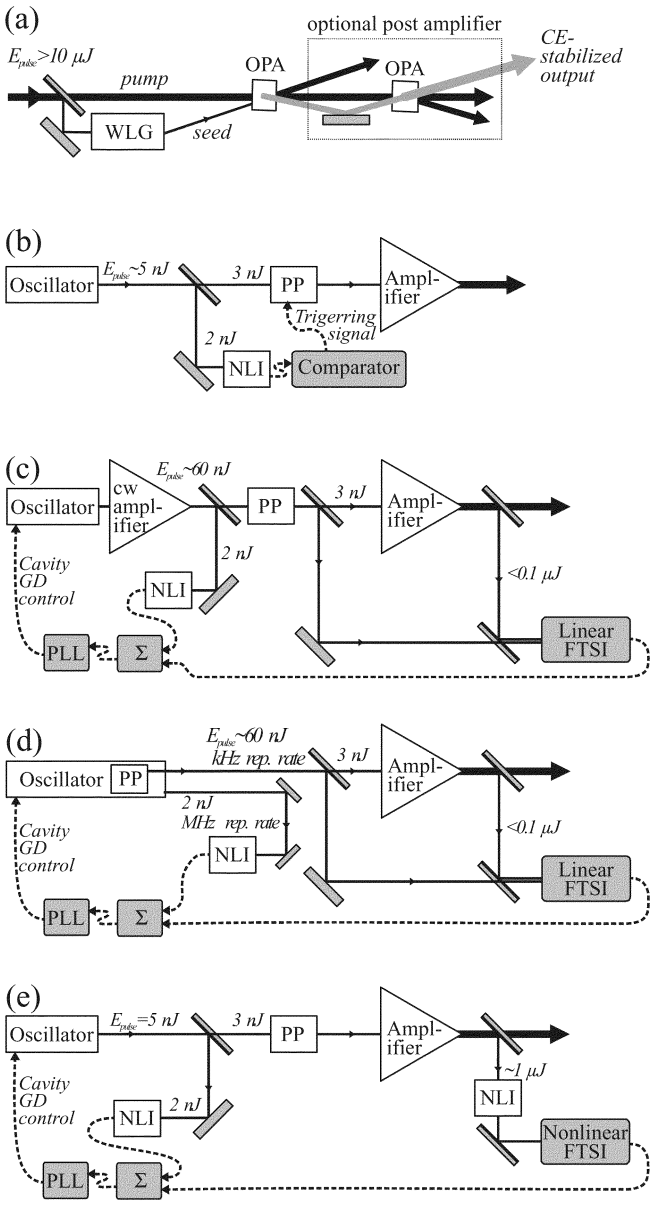

Fig. 6. Various concepts of phase-stable pulse amplification. (a) All-optical (passive) phase stabilization with an OPA. (b) Phase-selective seed by a free-running oscillator. (c), (d), (e) Schemes employing a phase-stabilized seed oscillator with a secondary phase correction loop behind the amplifier based on linear (c), (d) and nonlinear (e) phase drift detection. Concepts (c) and (d) require high-energy seed that can be attained with a cw-amplified or a long-cavity oscillator (c) and a cavity-dumped oscillator (d). PP, pulse picker. PLL, phase —ocked loop. NLI, nonlinear f-to-$2f$ interferometer. See text for further explanation.

frequency comb [66] and creating phase-coherent frequency-shifted pulse replicas [23].

V. Concepts of Phase-Controlled Amplification

In this section, we suggest several practical designs of CE phase-stabilized amplifiers. The corresponding schematics are sketched in Fig. 6 and can employ both CPA [70], [71] and optical parametric amplification (OPA) [72]–[74]. Two types of CE phase drift in amplifiers must be considered. The first kind of phase noise is associated with the fluctuations of the intensity-dependent nonlinear phase contribution. It can vary randomly from pulse to pulse as the result of pump energy fluctuations and, therefore, cannot be compensated with active phase stabilization loops. To minimize this problem, the value of the so-called B-integral [75] $\Psi(t) = k(\omega_0)n_2 \int I(t,z)dz$, i.e., the accumulated nonlinear phase, or SPM in the amplifier, should be on the order of π. This condition is fulfilled in typical CPA amplifiers. Recent measurements of time-domain interferometric cross correlation between seed-oscillator pulses and their amplified replicas have shown that the phase jitter at the output of a multipass Ti:sa amplifier lies below 0.1 rad [76]. In fact, with pump energy fluctuations being the chief contributor to the jitter of the nonlinear phase, the use of low-noise diode-pumped pump lasers should make it possible to phase-stabilize amplifiers operating at higher B-integral values.

The second kind of CE drift is caused by beam pointing instability that leads to path length fluctuations in dispersive elements [45] of the amplifier. Such mechanical perturbations occur on a relatively slow timescale, with characteristic time constants of 1 s or higher. Therefore, the respective CE phase modulation could be traced and (pre-)compensated rather easily.

The schemes of CE phase control amplification, discussed here, can be divided into three categories: 1) all-optical phase self-stabilization [Fig. 6(a)]; 2) passive triggering on a seed pulse with an appropriate CE phase value [Fig. 6(b)]; and 3) use of CE phase-stabilized seed with a sub-loop for phase correction of the amplifier output [Fig. 6(c)–(e)].

Recently, it has been shown that passive CE phase stabilization can be obtained in an appropriately configured OPA [23]. This is achieved by seeding the OPA with a white-light pulse that is generated by the OPA pump pulse. According to the considerations in Section IV, both the seed and the pump pulses are phase-coherent and, in the process of difference frequency generation (DFG), the phases of these two pulses add up with opposite signs. Therefore, the amplified idler pulse, which is a result of DFG between the pump and the seed, becomes free of CE drift even when the OPA is pumped with random-CE-phase pulses. This scheme, shown in Fig. 6(a), can be used as a phase-stabilizing extension of a conventional free-running CPA amplifier. Subsequent power amplification can be carried out by broad-band chirped-pulse OPA into a TW-PW regime [74]. The drawback of this approach is the red-shifted output wavelength of the idler wave, which does not permit the post-amplification to be carried out in the laser gain medium used to generate the pump beam. Consequently, implementation of all-optical phase stabilization in high-energy systems cannot be straightforward and demands development of dedicated amplification stages.

Other designs presented in Fig. 6(b) and (e) are intended as upgrades of existing amplified systems. Fig. 6(b) represents the simplest possible realization of phase control based on the fact that there is a 10^5 difference in the repetition rates of the seed oscillator and a kilohertz amplifier. It has been shown that the CE phase evolution of the oscillator pulse train is quasi-periodic [9], [14] and the rate of the pulse-to-pulse phase slippage $\Delta\varphi$ can be adjusted by manipulating the cavity dispersion. With an f-to-$2f$ interferometer [Fig. 2(a)], one can monitor the evolution of the ω_{CE} beat and employ this signal for triggering a pulse picker to select an oscillator pulse with a desired phase [14], [77]. To ensure proper amplification, the pulse picker must be triggered

shortly after the flash of the kilohertz pump laser and within the lifetime of population inversion, which leaves room to select an "appropriate" seed pulse from thousands of oscillator shots. The key drawback of this scheme is a relatively poor precision with which such a selection can be performed, since there could be up to several additional laser shots between the triggering pulse and the one actually sent to the amplifier. In this situation, variations of the quasi-periodic phase change would introduce a variable CE phase shift of the selected pulse. Another foreseen difficulty in this method is the lack of obvious mechanism to counter phase fluctuations arising from the amplifier itself.

The schemes drawn in Fig. 6(c) and (d) are based on the use of a CE-controlled seed oscillator [13], [14] and explore the possibility of sending a reference (pilot) beam for the measurement of the phase offset in the amplifier. The information on the slow phase drift behind the amplifier, obtained with the linear FTSI technique described in Section III-C, can then be plugged into the phase stabilization loop of the oscillator. The core of the phase stabilizing electronics is the phase-lock loop (PLL in Fig. 6), which forces the beat signal $\omega_{\rm CE}$ to oscillate in phase with an external local oscillator via a feedback to the intracavity dispersion. The inverse value of the phase offset measured by FTSI at the amplifier output can then be combined with the phase of the local oscillator signal $1/4\omega_{\rm rep}$, thus precompensating this offset already in the oscillator.

The use of the reference beam for (a potentially single-shot) FTSI imposes the demand for high seed pulse energy. Pulses of tens of nanojoules can be obtained by an intermediate continuous wave (cw) amplification of the seed pulse train before f-to-$2f$ characterization or by employing long-cavity oscillators [14], [78]. Another way to fulfill the pulse energy requirement is to use a cavity-dumped seed oscillator [79]–[81]. This type of laser has a dual output: through the output coupler it emits a pulse train at the full repetition rate, which can be conveniently used to drive the f-to-$2f$ interferometer, while the pulses ejected by the intracavity pulse picker are directly synchronized with the amplifier and satisfy the needs for a kilohertz seed and FTSI reference.

The remaining concept for phase control of an amplifier [Fig. 6(e)] offers the largest compatibility with existing CPA systems and is well suited for retrofitting them. This scheme requires implementation of a standard phase-lock loop of the seed oscillator (consisting of an f-to-$2f$ interferometer for the oscillator [Fig. 2(a)] and electronics) and addition of a secondary feedback loop (high-energy f-to-$2f$ interferometer and computer for FTSI). Importantly, neither the oscillator nor the amplifier needs to undergo significant modifications. As will be shown below, we have followed this blueprint to upgrade a standard multipass Ti:sapphire CPA system [52] for CE phase-stabilized operation.

VI. Phase-Stabilized 5-fs 0.1-TW Amplified System

In our high-power laser setup [Fig. 6(e)], we have incorporated a commercially available phase-stabilized 10-fs laser system (FS 800, Menlosystems GmbH). It consists of a dispersive-mirror-controlled Kerr-lens-mode-locked Ti:sapphire oscillator (Femtosource Compact Pro, Femtolasers GmbH), an f-to-$2f$ interferometer [Fig. 2(a)], and phase-locking electronics driving an acousto-optic modulator that controls the intensity of the cw pump laser (Verdi V, Coherent). About 50% of the output of the oscillator is diverted into a 2-cm-long photonic crystal fiber for the detection of the CE beat frequency $\omega_{\rm CE}$ [Fig. 2(a)]. The reference signal (i.e., the local oscillator) for the phase-locked loop is derived by dividing the repetition rate of the oscillator 80 MHz detected with the $\omega_{\rm CE}$ [detector shown in Fig. 2(a)] by a factor of 4. As can be readily understood from (3), selecting $\omega_{\rm rep}$ (or its (sub)harmonics as the reference signal) is the best choice to control the value of $\omega_{\rm CE}$. Before activating the phase-locked loop, we set the intracavity CE phase shift $\Delta\varphi$ approximately to $2\pi(m+1/4)$, where m is an integer. This rough adjustment of $\Delta\varphi$ is performed by changing the optical path length through a pair of thin intracavity wedges of fused silica. At this stage, φ is approximately reproduced in every fourth roundtrip in the laser cavity, which results in a quasi-periodic modulation of the f-to-$2f$ beat signal at a quarter repetition rate, i.e., 20 MHz. Next, to enhance the accuracy of the phase reproducibility, the $\omega_{\rm CE}$ (and $\omega_{\rm rep}/4$) are then phase-locked, which is achieved by controlling $\Delta\varphi$ via nonlinear effects in the Ti:sapphire crystal through the variation of the pump intensity [9]. For this purpose, the beam of the cw pump laser is passed through the acousto-optic modulator [14], [82], which varies the power of the transmitted beam accordingly to the phase error signal derived in the phase detector of the phase-lock loop [Fig. 6(c)–(e)]. As a result, every fourth pulse in the 80-MHz pulse train carries the same CE phase, giving rise to an accurate optical field reproduction.

In our current work, we have employed a multipass Ti:sapphire chirped-pulse amplifier (Femtopower, Femtolasers GmbH). The Q-switched diode-pumped pump laser (Corona, Coherent Inc.) of the amplifier and the pulse picker (Pockels cell) in the amplifier were synchronized with exactly every 80.000th pulse from the oscillator, which ensures that only pulses with identical φ are amplified (at a repetition rate of 1 kHz). The nanojoule pulses are temporally stretched by a glass block before their energy is boosted to $\approx$1 mJ in nine passes through a 4-mm-long Ti:sapphire crystal. After amplification, the duration of the pulses is reduced to $\approx$ 20 fs in a refractive pulse compressor consisting of two pairs of Brewster-angled prisms. To shorten the pulse even further, the output of the amplifier is injected into a 1-m-long hollow-core glass fiber filled with neon gas and subsequently passed through a set of ultrabroad-band chirped mirrors. To detect the CE phase variations, a small fraction ($<1\%$) of the energy of the 20-fs pulses is split off from the main beam directly behind the amplifier and fed into the second f-to-$2f$ interferometer sketched in Fig. 2(b), the working of which was discussed in Section III-B. The parameters of the resultant output pulses are summarized in Fig. 7(a). The insets in Fig. 7(a) depict the measured spectrum and second-order interferometric autocorrelation of the compressed pulses. An iterative pulse retrieval from these data [83] yields a near-bandwidth-limited pulse with an amplitude envelope $A_L(t)$ (shown by the thin dashed line in Fig. 7(a)] and a laser pulse duration (full width at the half maximum of $A_L(t)^2$) of $\tau_L = 5.4 \pm 0.5$ fs.

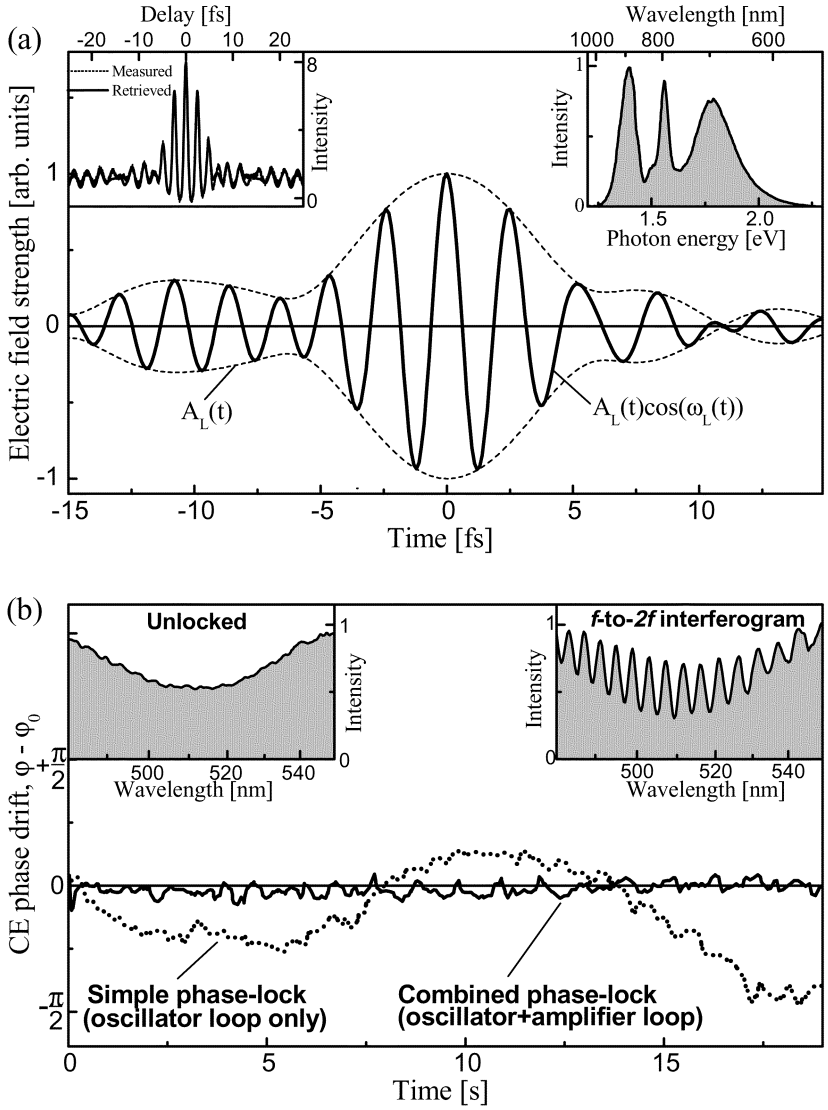

Fig. 7. Performance overview of the phase-stabilized amplified system. (a) Pulse properties behind the hollow-fiber-chirped-mirror compressor. Retrieved pulse envelope (dashed curves) and a possible electric field (solid curve) of the compressed pulse. Insets show measured intensity spectrum (right) and measured and retrieved second-order interfrometric autocorrelation (left). (b) Carrier-envelope phase dynamics with oscillator-only phase stabilization (dotted curve) and combined oscillator-amplifier phase stabilization (solid curve). Insets show f-to-$2f$ interference spectrograms recorded with the nonlinear interferometer at the amplifier output [Fig. 6(e)].

Experimental results, obtained with the second f-to-$2f$ interferometer in different phase stabilization regimes of the amplifier, are summarized in Fig. 7(b). In the case of a phase-unlocked seed oscillator, the interference pattern is completely averaged out within approximately 200 laser shots (black curve, left inset of Fig. 7(b), which signifies the importance of the single-shot capability of monitoring the φ drift. By strong contrast, seeding the amplifier system with phase-locked pulses preserves a clear interference pattern for CCD exposure times as long as several seconds without any further stabilization other than that performed by tracing the ω_{CE} at the oscillator output. The temporal evolution of the CE phase variation in this mode, which we term simple phase-lock, is exemplified in Fig. 7(b) by the dotted curve. These data reveal that the CE phase of the high-energy 20-fs pulses remains virtually stable for periods up to several seconds long. This is remarkable considering the sensitivity of the CE phase to the path length change in any solid optical medium [9]. Beam direction instabilities in the microradian range can produce path-length changes of this order of magnitude in the prism compressor and are likely to provide a significant contribution to the phase drifts on a longer time scale. It is important to point out that, compared with other femtosecond amplifiers employing long pulse diffraction-grating-based stretchers, our system presents a clear advantage in terms of angular beam stability as the result of employing a bulk-material pulse chirping.

The slow drift of φ shown by the dotted curve in Fig. 7(b) can be readily tracked by computer analysis of the f-to-$2f$ fringe pattern [right inset in Fig. 7(b)]. A voltage proportional to the change of φ is generated by a personal computer that performs the FTSI analysis of the f-to-$2f$ interferograms. As shown in Fig. 6(e), this signal is combined with the fast-changing feedback from the first f-to-$2f$ unit that monitors the phase evolution of the seed oscillator. The absence of fast phase

changes in the amplifier allows us to accumulate the interferograms measured in the second nonlinear interferometer [Fig. 2(b)] for about 20–30 ms (i.e., 20–30 laser shots). The implementation of this signal integration smoothens the operation of the feedback loop by preventing accidental overshoots of the CE phase control. Once stabilized at a certain value of φ, the phase behind the amplifier can be controlled with the FTSI computer by adding an offset value to the feedback signal. The simultaneous use of both feedback loops allows stabilizing the phase for extended periods ($\gg$1 min). The solid curve in Fig. 7(b) shows the typical phase drift measured in the second f-to-$2f$ device with both feedbacks active and exhibits an rms jitter of ~ 75 mrad. This figure, however, should not be confused with the actual precision, with which the CE phase can be maintained behind the amplifier. Since the phase characterization in the nonlinear interferometer is influenced by the device noise (cf. discussion in Section III), the feedback loop would not be able to discriminate this measurement noise from the real phase jitter in the amplifier. Therefore, an external (out-of-loop) experiment is required to confirm the CE phase stability and will be presented in Section VII.

An important point that has not been addressed so far is the CE phase stability of the pulses passing the hollow waveguide that is used to obtain the spectral broadening shown in the right inset to Fig. 7(a). We have purposely placed the second f-to-$2f$ interferometer behind the amplifier rather than at the output of the hollow-fiber-chirped-mirror compressor. The reason for that is a better intensity stability of the 20-fs pulses (around 1% rms). The intensity noise of the white light emerging from the fiber is higher and varies from 1.6% rms in the spectral region of the input laser pulse to 4% at 650 nm. At the same time, the spectral breadth of this white-light continuum is insufficient to support an f-to-$2f$ detection under the optimal conditions for the generation of 5-fs pulses. To assess the detrimental effect of the hollow-fiber WLG on the CE phase stability, we repeated the experiments described in Section IV (Fig. 4). The resultant pulse-to-pulse rms phase noise was found to range from 80 to 140 mrad, depending on the pressure of neon in the capillary. We also conducted intensity dependence measurements of the phase offset within a $\pm 15\%$ energy range around the mean energy value (700 μJ) injected into the fiber. This study revealed a 3.4 mrad/μJ slope dependence of the phase change within the region of spectral overlap between the laser pulse and the white light. Unfortunately, with the FTSI method, it is impossible to assess the phase jitter across the whole spectrum of the continuum. Nevertheless, one cannot expect dramatic phase excursions in the spectral wings since they would have an immediate impact on the pulse profile. Such envelope fluctuations of the compressed pulse have not been observed in our system. The results of the FTSI measurements presented above justify the use of the f-to-$2f$ detection in front of the hollow fiber.

VII. Control of Light Field Oscillations

The reference phase in the combined feedback loop of our high-power phase-controlled laser system can be adjusted within a range of 2π, providing a convenient means of setting φ equal to an arbitrary value. Nevertheless, as has been pointed out above, the techniques that we have implemented so far merely enable us to keep φ constant and vary it by a known amount, whereas the actual value of φ remains undisclosed. As opposed to the f-to-$2f$ technique, strong field phenomena driven by few-cycle pulses have been predicted to be sensitive to φ and potentially could serve for its determination. The processes predicted to be suitable for this purpose include high-order harmonic emission [33], [34], [84] and above-threshold ionization [37], [42], [43], [85], [86]. Here, we chose high-order harmonic generation as the subject of our investigations because it has a relatively simple experimental implementation and relies on linearly polarized light readily available in our setup. In addition, a clear intuitive insight into this process had been developed in several excellent models [25], [26], [87] that have been tested and confirmed by a large number of numerical studies and experiments [32]–[34], [88].

The relevant aspects of the process can be summarized as follows. The highest energy XUV or soft-X-ray photons are emitted around the zero transition(s) of the laser electric field near the peak of the pulse. This is implicit in semiclassical models [6], [25], [26], [87] and was recently verified in an attosecond experiment [30]. The energy of the emitted photon is essentially determined by the intensity of the laser half-cycle preceding the emission. For a few-cycle pulse with $\varphi \approx 0$ or π [the so-called "cosine" wave, shown in Fig. 1(b)] there is only one single most intense half cycle, which implies the emission of an isolated X-ray burst at the highest photon energies [Fig. 1(h)]. The presence of such an isolated feature in the time domain corresponds to a smooth spectrum. By a stark contrast, an identical pulse with a "sine" carrier ($\varphi \approx \pm\pi/2$, Fig. 1(c) exhibits two most intense half cycles, giving rise to a pair of soft-X-ray bursts separated by $T_0/2$ in time [Fig. 1(i)]. In the frequency domain, this temporal structure implies a modulated (quasi-harmonic) spectrum up to the highest photon energies.

In order to check the validity of this simple intuitive picture we have developed a computer code simulating propagation of an intense few-cycle laser pulse through an ionizing medium. The program solves Maxwell's equations in three space dimensions and calculates the emergence of high-order harmonics using a refined version [6] of the quantum theory of Lewenstein *et al.* [26], [89]. Fig. 8 summarizes the results of the simulations relevant to the experiments described as follows: laser pulse duration: $\tau_L = 5$ fs, pulse energy: 0.2 mJ, beam diameter: $2w_L = 122$ μm; medium: neon, pressure: 100 mbar, length: 2 mm. Fig. 8(a)–(d) displays the computed spectral distribution of few-cycle-driven coherent soft-X-ray emission from neon in the cutoff range for four different values of the CE phase of the driver laser pulse. Fig. 8(e) and (f) shows the temporal intensity profile of cutoff X-rays transmitted through a Gaussian filter [solid contour in Fig. 8(a)] for $\varphi = 0$ and $\varphi = \pi/2$ (solid curves) along with the instantaneous intensity of driving laser (i.e., $E_L(t)^2$) depicted by dashed curves. It should be noted that detailed numerical simulations show that the smoothest and the most modulated spectral cutoff features actually correspond to the values of $\sim 20^\circ$ and $\sim 110^\circ$, respectively, rather than to the intuitively anticipated values of 0° and 90°. This discrepancy, however, is insignificant in our experiments since it lies within the uncertainty with which we can identify different CE phase values.

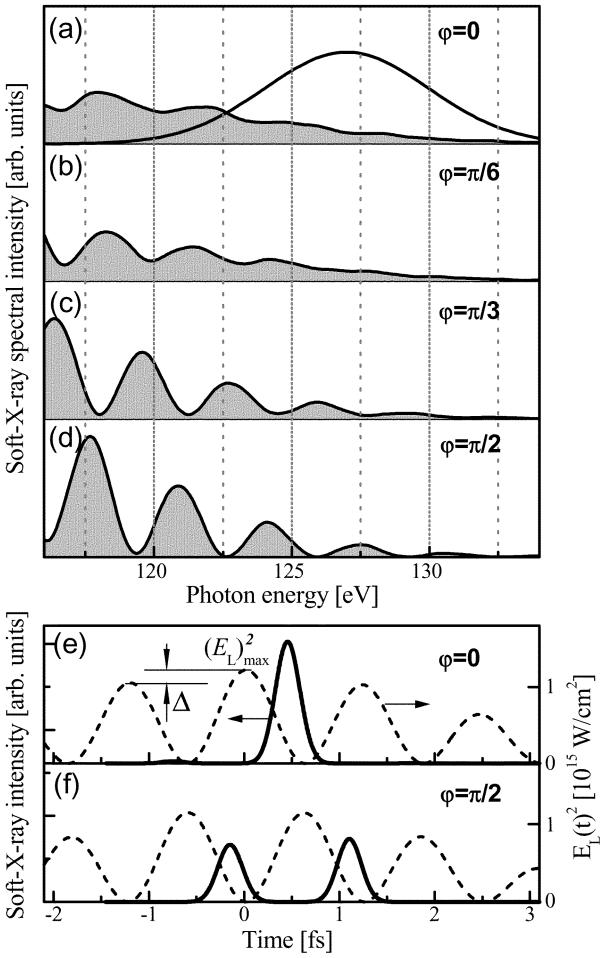

Fig. 8. Numerical simulations of few-cycle-driven coherent soft-X-ray emission from ionizing atoms. (a)–(d) Cutoff-range spectra for different CE phase settings of the driving laser pulse. (e)–(f) Solid curves depict the temporal intensity profile of the cutoff harmonic radiation filtered through a Gaussian bandpass filter with a full-width at half maximum of 7 eV [solid contour in (a)], whereas the dashed curves plot $E_L(t)^2$. These results support the intuitive analysis: the field carrying $\varphi = 0$ is predicted to produce a single soft-X-ray burst [filtered in the cutoff, (e)]. Deviation of φ from zero gradually suppresses the magnitude of the main burst and gives rise to a satellite spike. Latter becomes most prominent for $|\varphi| \rightarrow \pi/2$ (f). In the frequency domain, the isolated pulse emerging for $\varphi = 0$ implies a continuous spectrum shown in (a), which becomes increasingly modulated with the appearance of the second burst for $|\varphi| \rightarrow \pi/2$ (b)–(d).

The results of simulations, presented above, along with previous numerical studies [6], [33], [34], [90] fully support our intuitive analysis and show a strong spectral dependence between the temporal structure of the X-ray bursts and the spectral shape of the cutoff region. The width of the smoothened spectral part (continuum), $\Delta(\hbar\omega)_{\rm cont}$, that corresponds to an isolated X-ray burst, depends on the ratio of instantaneous intensity $E_L(t)^2$ of the strongest half cycle and its neighboring peak. The corresponding difference of instantaneous intensity is marked by Δ in Fig. 8(e). Because of the linear dependence between the highest emitted X-ray photon energy and the peak laser intensity, the continuum bandwidth can be expressed as follows:

$$\Delta(\hbar\omega)_{\rm cont} = \frac{\hbar\omega_{\rm cutoff} - I_p}{(E_L(t)^2)_{\rm max}}\Delta \qquad (11)$$

where I_p is the ionization potential. Table I lists the instantaneous intensity ratio and the width of the continuum (calculated at 125 eV) for several values of τ_L/T_0, which is the number of oscillation cycles within the laser pulse duration.

TABLE I
EXPECTED SPECTRAL WIDTH OF THE CUTOFF CONTINUUM FOR A $\varphi = 0$ WAVE AS A FUNCTION OF PULSE DURATION. SEE TEXT AND FIG. 8 FOR DEFINITION OF PARAMETERS

τ_L/T_0	$\Delta/\left(E_L(t)^2\right)_{max}$	$\Delta(\hbar\omega)_{cont}$@125eV
2	0.16	20 eV
3	0.07	8.8 eV
4	0.04	5.0 eV
5	0.03	3.8 eV

According to the data in Table I, $\tau_L/T_0 \leq 2.5$ is required to produce a continuum with a sizeable $(>10$ eV$)$ bandwidth in the 100-eV range. For few-cycle pulses that comply with this demand, the appearance of the predicted continuum [Fig. 8(a)] is a robust feature appearing for a broad range of parameters as long as the propagation length does not exceed half the coherence length [6]. Experimentally, this condition is readily fulfilled by operating the high-harmonic source at a gas density equal to or below that resulting in maximum cutoff yield. We generated high-order harmonics by gently focusing 5-fs 0.2-mJ laser pulses into a 2-mm-long neon gas medium. The cycle-averaged peak intensity was estimated to be 7×10^{14} W/cm^2. The neon gas was supplied in a thin-walled metal tube [35] with a backing pressure of 160 mbar. The pressure in the interaction region, however, was somewhat lower due to the gas expansion into the surrounding vacuum chamber. Thin zirconium foils were installed in the pathway of the emitted soft-X-ray radiation in order to block the laser light as well as low-order harmonics. The high-energy part of the spectrum (above 80 eV) was spectrally analyzed with a simple spectrometer consisting of a 10 000-line/mm transmission grating and a backside-illuminated soft-X-ray CCD camera (Roper Scientific).

Fig. 9 shows a series of soft-X-ray spectra generated under the conditions described above for different values of the CE phase of the 5-fs pump pulses. For settings of $\varphi = \varphi_0$, the harmonics near the cutoff $(\hbar\omega > 120$ eV$)$ completely merge to a continuum. Notably, with a gradual change of the phase, the continuous spectral distribution of the cutoff radiation begins to break up into discrete harmonic peaks, with the maximum modulation depth appearing for settings of $\varphi = \varphi_0 \pm \pi/2$. This behavior is in agreement with the above intuitive picture and computer simulations under the assumption of $\varphi_0 = 0 + n\pi$, where $n = 0, 1$. The residual ambiguity in the determination of φ relates to the inversion symmetry of the interaction with the atomic gas medium. A π-shift in φ results in no change of the light waveform other than reversing the direction of the electromagnetic field vectors. In an isotropic medium, such a phase flip cannot lead to any measurable physical consequences.

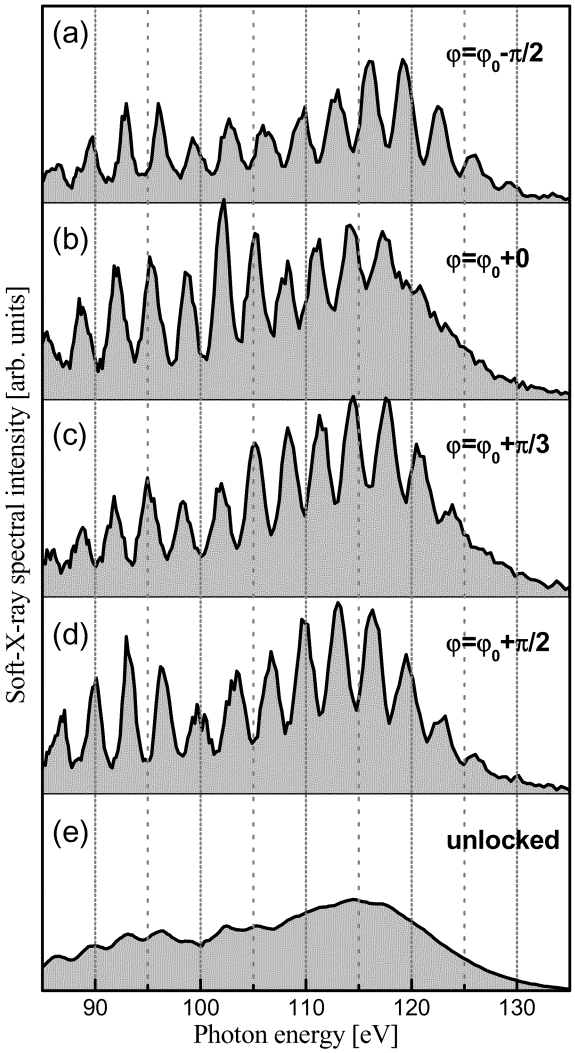

Fig. 9. Measured spectral intensity of soft-X-ray emission from ionizing atoms driven by 5-fs pulses. (a)–(d) Data obtained with phase-stabilized pulses for different CE phase settings. (e) Spectrum measured without CE phase stabilization. X-ray CCD exposure was 0.5 s in all cases.

The presence of the distinct spectral behavior in the cutoff region allows us to calibrate the actual value of the CE phase. A continuum with a bandwidth of ≈ 16 eV is clearly visible in Fig. 9(b) and is in fair agreement with the value of $\Delta(\hbar\omega)_{\rm cont} = 20$ eV predicted by our simple considerations for 5-fs 750-nm $(\tau_L/T_0 = 2)$ light pulses (Table I). The X-ray spectra corresponding to the phase settings shifted by $\pm\pi/2$ [Fig. 9(a) and (d)] on the contrary display a pronounced modulation surviving into the cutoff. Therefore, the CE phase can be evaluated with the highest possible accuracy by recording pairs of soft-X-ray harmonic spectra at $\varphi_1 = \varphi$ and $\varphi_2 = \varphi + \pi/2$, where φ is varied in small steps. In this method, $\varphi = 0$ (or, equivalently, π) can be identified from a pair of spectra that exhibit, respectively, the smallest and the largest modulation depth in the cutoff range. Applying this procedure to the data in Fig. 9, we conclude that the phase setting $\varphi_0 \approx 0$. The current amplitude and phase stability of our source permits identification of the CE phase value with an accuracy better than $\pi/5$. The obtained value of φ is subsequently used to calibrate the interference pattern recorded in the second f-to-$2f$ interferometer. After performing this calibration, we can subsequently change φ with an accuracy better than $\pi/10$ using the interferometer.

Another noteworthy feature that has emerged from the soft-X-ray experiments with phase-stabilized pulses is the shift of the harmonic peaks with φ. This effect has been predicted by previous [34], [91] as well as by our current simulations and clearly manifests itself in the spectra shown in Fig. 9. This shift indicates that the peaks visible in the few-cycle-driven harmonic spectra, strictly speaking, do not represent genuine harmonics, because the laser frequency is kept unchanged and so its harmonics are expected to remain invariant as well. The shift of these "quasi-harmonics" is a direct consequence of the variation of the field amplitude within T_0 and the confinement of emission within only a couple of oscillation cycles. This CE-phase-induced shift completely smears the harmonic structure of the near-cutoff soft X-rays generated by our 5-fs pulses in the absence of phase stabilization [Fig. 9(e)].

To gain further insight into this effect of spectral shift and smearing, we have recorded X-ray spectra obtained with longer laser pulses. The pulse duration was lengthened to about 10 fs and the energy of the pulses sent to the target was increased in order to reach the same cutoff frequency as in the data in Fig. 9. The obtained spectra are displayed in Fig. 10 and exhibit several differences with respect to the 5-fs case. First, there is no pronounced continuum in the cutoff region that would permit identification of the φ_0 phase offset, as is expected for this pulse width in accordance with Table I. Second, there are clear spectral peaks at photon energies up to 110 eV that survive even into the phase-unlocked regime (Fig. 10, bottom panel). The blow-up in Fig. 10(b) shows that the frequencies of these peaks do not vary with phase and, consequently, they represent true odd-number harmonic orders of the laser field. However, the situation is dramatically changed toward the cutoff because the spectral peaks seen there [Fig. 10(c)] shift their frequency by the full laser photon energy. A similar behavior has been observed recently by another group of researchers who detected single-shot X-ray spectra with a CE phase-unlocked laser [92]. Apparently, such a quasi-periodic spectral pattern is the result of a complicated interference interplay among X-rays bursts generated by a laser field the amplitude of which changes significantly within an optical cycle [90]. The "true" harmonics at low frequencies are produced by many participating peaks of the laser field, whereas the "false" harmonics, approaching the cutoff, are formed by very few field peaks. In this regard, it is interesting to note the anomaly in the energy interval of 95–105 eV in Fig. 10. This "intermediate" region features quasi-harmonic peaks with a period of one laser photon energy. This is remarkable, since such periodicity corresponds to laser field peaks separated by T_0 rather than by the usual $T_0/2$ (i.e., by the time spacing between the nearest half cycles). In our understanding, the reason for this transient behavior is the involvement of three neighboring half cycles capable of generating X-rays at that frequency, a condition that cannot be fulfilled at both lower and higher photon energies.

Both the experiments with 5- and 10-fs pulses, described in this section, signify the great benefits that CE phase stabilization brings to the study of coherent laser-driven X-ray sources.

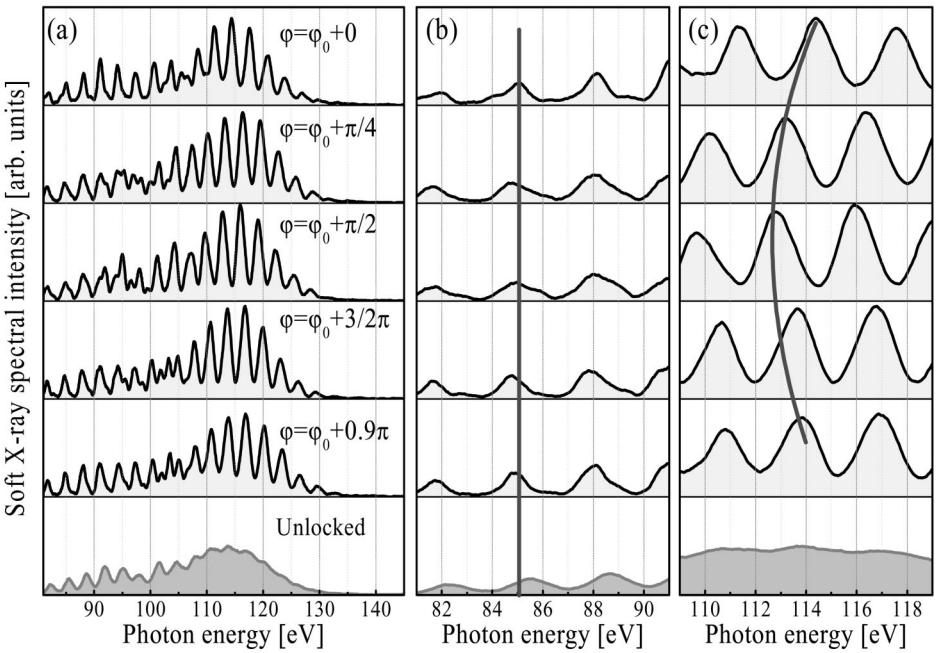

Fig. 10. Measured spectral intensity of soft-X-ray emission from ionizing atoms driven by 10-fs pulses. (a) Full-range spectra. (b), (c) Close-ups on spectral regions with distinctly different spectral dependencies on CE phase.

VIII. Conclusion and Outlook

In this work, we have demonstrated the generation of intense few-cycle light pulses with a reproducible temporal evolution of the electromagnetic field. With these light waveforms we have explored the sensitivity of microscopic atomic currents to the timing of light field oscillations with respect to the pulse peak. The short-wavelength (XUV, soft-X-ray) radiation emitted by the atomic currents has allowed determination of this timing with sub-$T_0/10$ (i.e., sub-250 as) accuracy. The generation of intense few-cycle light with a reproducible and known waveform is expected to benefit the emerging field of attosecond physics in several ways.

The high-frequency atomic currents, employed as a light-waveform detector in the current experiments, are also sources of subfemtosecond XUV/soft-X-ray pulses [27]–[30]. Therefore, the measurement and stabilization of the CE phase presented in this research directly opens the way to generate single isolated subfemtosecond pulses that are ideally suited for most spectroscopic applications. Ultrashort wavepackets with controlled field oscillations will also benefit the techniques that have been recently introduced for attosecond metrology [29], [30] and attosecond spectroscopy [31]. They are indispensable to measuring the shape and chirp of subfemtosecond XUV or X-ray pulses [93], [94] and to observing inner-shell atomic processes on an attosecond timescale [31]. Last but not least, control over the temporal structure of electron wave packets liberated by optical-field ionization also relies on synthesized light waveforms. Few-cycle light with controlled field oscillations will be able to launch an electron wave packet with well-controlled subfemtosecond temporal structure into the continuum and precisely steer its subsequent motion. One intriguing scenario is to make the electron recollide with its parent ion and use this recollision to excite and/or probe molecular [95], [96], atomic, or possibly even nuclear dynamics. Finally, yet another potential application area of high-intensity waveforms is electron acceleration in the forward direction to ultrarelativistic energies in a highly controlled manner.

References

[1] A. Weiner, "Femtosecond pulse shaping using spatial light modulators," *Rev. Sci. Instrum.*, vol. 71, pp. 1929–1960, 2000.

[2] R. Trebino, K. DeLong, D. Fittinghoff, J. Sweetser, M. Krumbugel, B. Richman, and D. Kane, "Measuring ultrashort laser pulses in the time-frequency domain using frequency-resolved optical gating," *Rev. Sci. Instrum.*, vol. 68, pp. 3277–3295, 1997.

[3] C. Iaconis and I. A. Walmsley, "Spectral phase interferometry for direct electric-field reconstruction of ultrashort optical pulses," *Opt. Lett.*, vol. 23, pp. 792–794, 1998.

[4] E. Constant, "Champs laser intenses ultracourts: Application à la mesure et création d'impulsions attosecondes et à l'imagerie de paquets d'ondes moléculaires par explosion coulombienne," Ph.D. dissertation, Univ. Sherbrooke, Sherbrooke, QC, Canada, 1997.

[5] G. Steinmeyer, D. Sutter, L. Gallmann, N. Matuschek, and U. Keller, "Frontiers in ultrashort pulse generation: Pushing the limits in linear and nonlinear optics," *Science*, vol. 286, pp. 1507–1512, 1999.

[6] T. Brabec and F. Krausz, "Intense few-cycle laser fields: Frontiers of nonlinear optics," *Rev. Mod. Phys.*, vol. 72, pp. 545–591, 2000.

[7] A. Baltuška, T. Fuji, and T. Kobayashi, "Visible pulse compression to 4 fs by optical parametric amplification and programmable dispersion control," *Opt. Lett.*, vol. 27, pp. 306–308, 2002.

[8] B. Schenkel, J. Biegert, U. Keller, C. Vozzi, M. Nisoli, G. Sansone, S. Stagira, S. De Silvestri, and O. Svelto, "Generation of 3.8-fs pulses from adaptive compression of a cascaded hollow fiber supercontinuum," *Opt. Lett.*, 2003, to be published.

[9] L. Xu, C. Spielmann, A. Poppe, T. Brabec, F. Krausz, and T. W. Hänsch, "Route to phase control of ultrashort light pulses," *Opt. Lett.*, vol. 21, pp. 2008–2010, 1996.

[10] T. Udem, "Phasenkohärente optische frequenzmessungen am wasserstoffatom," Ph.D. dissertation, Ludwig-Maximilians Universität, Munich, Germany, 1997.

[11] J. Reichert, R. Holzwarth, T. Udem, and T. W. Hänsch, "Measuring the frequency of light with mode-locked lasers," *Opt. Commun.*, vol. 172, p. 59, 1999.

[12] H. R. Telle, G. Steinmeyer, A. E. Dunlop, J. Stenger, D. H. Sutter, and U. Keller, "Carrier-envelope offset phase control: A novel concept for absolute optical frequency measurement and ultrashort pulse generation," *Appl. Phys. B.*, vol. 69, pp. 327–332, 1999.

[13] D. J. Jones, S. A. Diddams, J. K. Ranka, A. Stentz, R. S. Windeler, J. L. Hall, and S. T. Cundiff, "Carrier-Envelope phase control of femtosecond mode-locked lasers and direct optical frequency synthesis," *Science*, vol. 288, pp. 635–639, 2000.

[14] A. Apolonski, A. Poppe, G. Tempea, C. Spielmann, T. Udem, R. Holzwarth, T. W. Hänsch, and F. Krausz, "Controlling the phase evolution of few-cycle light pulses," *Phys. Rev. Lett.*, vol. 85, pp. 740–743, 2000.

[15] T. Udem, J. Reichert, R. Holzwarth, and T. W. Hänsch, "Accurate measurement of large optical frequency differences with a mode-locked laser," *Opt. Lett.*, vol. 24, pp. 881–883, 1999.

[16] R. Holzwarth, T. Udem, T. W. Hänsch, J. C. Knight, W. J. Wadsworth, and P. S. J. Russel, "Optical frequency synthesizer for precision spectroscopy," *Phys. Rev. Lett.*, vol. 85, pp. 2264–2267, 2000.

[17] S. A. Diddams, D. J. Jones, J. Ye, T. Cundiff, and J. L. Hall, "Direct link between microwave and optical frequencies with a 300 THz femtosecond laser comb," *Phys. Rev. Lett.*, vol. 84, pp. 5102–5105, 2000.

[18] S. T. Cundiff, J. Ye, and J. L. Hall, "Optical frequency synthesis based on mode-locked lasers," *Rev. Sci. Instrum.*, vol. 72, pp. 3749–3771, 2001.

[19] S. T. Cundiff, "Phase stabilization of ultrashort optical pulses," *J. Phys. D: Appl. Phys.*, vol. 35, pp. R43–R59, 2002.

[20] T. Udem, R. Holzwarth, and T. W. Hänsch, "Optical frequency metrology," *Nature*, vol. 416, pp. 233–237, 2002.

[21] MenloSystems GmbH. [Online]. Available: http://www.menlosystems.com/

[22] M. Kakehata, H. Takada, Y. Kobayashi, K. Torizuka, Y. Fujihara, T. Homma, and H. Takahashi, "Single-shot measurement of carrier-envelope phase changes by spectral interferometry," *Opt. Lett.*, vol. 26, pp. 1436–1438, 2001.

[23] A. Baltuška, T. Fuji, and T. Kobayashi, "Controlling the carrier-envelope phase of ultrashort light pulses with optical parametric amplifiers," *Phys. Rev. Lett.*, vol. 88, pp. 133 901/1–4, 2002.

[24] ——, "Self-referencing of the carrier-envelope slip in a 6-fs visible parametric amplifier," *Opt. Lett.*, vol. 27, pp. 1241–1243, 2002.

[25] P. B. Corkum, "Plasma perspective on strong-field multiphoton ionization," *Phys. Rev. Lett.*, vol. 71, pp. 1994–1997, 1993.

[26] M. Lewenstein, P. Balcou, M. Y. Ivanov, A. L'Huillier, and P. B. Corkum, "Theory of high-harmonic generation by low-frequency laser fields," *Phys. Rev. A*, vol. 49, pp. 2117–2132, 1994.

[27] M. Drescher, M. Hentschel, R. Kienberger, G. Tempea, C. Spielmann, G. A. Reider, P. B. Corkum, and F. Krausz, "X-ray pulses approaching the attosecond frontier," *Science*, vol. 291, pp. 1923–1927, 2001.

[28] P. M. Paul, E. S. Toma, P. Breger, G. Mullot, F. Augé, P. Balcou, G. H. Muller, and P. Agostini, "Observation of a train of attosecond pulses from high harmonic generation," *Science*, vol. 292, pp. 1689–1692, 2001.

[29] M. Hentschel, R. Kienberger, C. Spielmann, G. A. Reider, N. Milosevic, T. Brabec, P. Corkum, U. Heinzmann, M. Drescher, and F. Krausz, "Attosecond metrology," *Nature*, vol. 414, pp. 509–513, 2001.

[30] R. Kienberger, M. Hentschel, M. Uiberacker, C. Spielmann, M. Kitzler, A. Scrinzi, M. Wieland, T. Westerwalbesloh, U. Kleineberg, U. Heinzmann, M. Drescher, and F. Krausz, "Steering attosecond electron wave packets with light," *Science*, vol. 297, pp. 1144–1148, 2002.

[31] M. Drescher, M. Hentschel, R. Kienberger, M. Uiberacker, V. Yakovlev, A. Scrinzi, T. Westerwalbesloh, U. Kleineberg, U. Heinzmann, and F. Krausz, "Time-resolved atomic inner-shell spectroscopy," *Nature*, vol. 419, pp. 803–807, 2002.

[32] I. P. Christov, M. M. Murnane, and H. C. Kapteyn, "High-Harmonic generation of attosecond pulses in the open-quotes single-cycleclose quotes regime," *Phys. Rev. Lett.*, vol. 78, pp. 1251–1254, 1997.

[33] A. de Bohan, P. Antoine, D. B. Miloševic, and B. Piraux, "Phase-dependent harmonic emission with ultrashort laser pulses," *Phys. Rev. Lett.*, vol. 81, pp. 1837–1840, 1998.

[34] G. Tempea, M. Geissler, and T. Brabec, "Phase sensitivity of high-order harmonic generation with few-cycle laser pulses," *J. Opt. Soc. Amer. B*, vol. 16, pp. 669–673, 1999.

[35] C. Spielmann, H. Burnett, Z. Sartania, R. Koppitsch, M. Schnürer, C. Kan, M. Lenzner, P. Wobrauschek, and F. Krausz, "Generation of coherent X-rays in the water window using 5-femtosecond laser pulses," *Science*, vol. 278, pp. 661–664, 1997.

[36] C. G. I. Durfee, A. R. Rundquist, S. Backus, C. Herne, M. M. Murnane, and H. C. Kapteyn, "Phase matching of high-order harmonics in hollow waveguides," *Phys. Rev. Lett.*, vol. 83, pp. 2187–2190, 1999.

[37] G. G. Paulus, F. Grabson, H. Walther, P. Villoresti, M. Nisoli, S. Stagira, E. Priori, and S. De Silvestri, "Absolute-phase phenomena in photoionization with few-cycle laser pulses," *Nature*, vol. 414, pp. 182–184, 2001.

[38] C. Lemell, X. M. Tong, F. Krausz, and J. Burgdörfer, "Electron emission from metal surfaces by ultrashort pulses: Determination of the carrier-envelope phase," *Phys. Rev. Lett.*, vol. 90, pp. 076 403/1–4, 2003.

[39] V. S. Yakovlev, P. Dombi, G. Tempea, C. Lemell, J. Burgdörfer, T. Udem, and A. Apolonski, "Phase-stabilized 4-fs pulses at the full oscillator repetition rate for a photoemission experiment," *Appl. Phys. B.*, vol. 76, pp. 329–332, 2003.

[40] A. Poppe, R. Holzwarth, A. Apolonski, G. Tempea, C. Spielmann, T. W. Hänsch, and F. Krausz, "Few-cycle optical waveform synthesis," *Appl. Phys. B*, vol. 72, pp. 373–376, 2001.

[41] Y. Kobayashi and K. Torizuka, "Measurement of the optical phase relation among subharmonic pulses in a femtosecond optical parametric oscillator," *Opt. Lett.*, vol. 25, pp. 856–858, 2000.

[42] P. Dietrich, F. Krausz, and P. B. Corkum, "Determining the absolute carrier phase of a few-cycle laser pulse," *Opt. Lett.*, vol. 25, pp. 16–18, 2000.

[43] I. P. Christov, "Phase-dependent loss due to nonadiabatic ionization by sub-10-fs pulses," *Opt. Lett.*, vol. 24, pp. 1425–1427, 1999.

[44] A. Baltuška, T. Udem, M. Uiberacker, M. Hentschel, E. Goulielmakis, C. Gohle, R. Holzwarth, V. S. Yakovlev, A. Scrinzi, T. W. Hänsch, and F. Krausz, "Attosecond control of electronic processes by intense light fields," *Nature*, vol. 421, pp. 611–615, 2003.

[45] G. Steinmeyer, "New approaches to the generation and characterization of few-cycle laser pulses," Habilitational, Inst. Quantum Electronics, Ultrafast Laser Physics, ETH Zürich, Zürich, Switzerland, 2001.

[46] U. Morgner, R. Ell, G. Metzler, T. R. Schibli, F. X. Kärtner, J. G. Fujimoto, H. A. Haus, and E. P. Ippen, "Nonlinear optics with phase-controlled pulses in the sub-two-cycle regime," *Phys. Rev. Lett.*, vol. 86, pp. 5462–5465, 2001.

[47] J. C. Knight, T. A. Birks, P. S. J. Russell, and D. M. Atkin, "All-silica single-mode optical fiber with photonic crystal cladding," *Opt. Lett.*, vol. 21, pp. 1547–1549, 1996.

[48] J. K. Ranka, R. S. Windeler, and A. J. Stentz, "Visible continuum generation in air-silica microstructure optical fibers with anomalous dispersion at 800 nm," *Opt. Lett.*, vol. 25, pp. 25–27, 2000.

[49] ——, "Optical properties of high-delta air-silica microstructure fibers," *Opt. Lett.*, vol. 25, p. 796, 2000.

[50] R. Ell, U. Morgner, F. X. Kärtner, J. G. Fujimoto, E. P. Ippen, V. Scheuer, G. Angelow, T. Tschudi, M. J. Lederer, A. Boiko, and B. Luther-Davies, "Generation of 5-fs pulses and octave-spanning spectra directly from a tisapphire laser," *Opt. Lett.*, vol. 26, pp. 373–375, 2001.

[51] A. Bartels and H. Kurz, "Generation of a broadband continuum by a tisapphire femtosecond oscillator with a 1-GHz repetition rate," *Opt. Lett.*, vol. 27, pp. 1839–1841, 2002.

[52] S. Sartania, Z. Cheng, M. Lenzner, G. Tempea, C. Spielmann, and F. Krausz, "Generation of 0.1-TW 5-fs optical pulses at a 1-kHz repetition rate," *Opt. Lett.*, vol. 22, pp. 1562–1564, 1997.

[53] M. Takeda, H. Ina, and S. Kobayashi, "Fourier-transform method of fringe-pattern analysis for computer-based topography and interferometry," *J. Opt. Soc. Amer.*, vol. 72, p. 156, 1982.

[54] C. Dorrer and F. Salin, "Characterization of spectral phase modulation by classical and polarization spectral interferometry," *J. Opt. Soc. Amer. B*, vol. 15, pp. 2331–2337, 1998.

[55] C. Dorrer, "Influence of the calibration of the detector on spectral interferometry," *J. Opt. Soc. Amer. B*, vol. 16, pp. 1160–1168, 1999.

[56] C. Dorrer, N. Belabas, J.-P. Likforman, and M. Joffre, "Experimental implementation of fourier-transform spectral interferometry and its application to the study of spectrometers," *Appl. Phys. B*, vol. 70, pp. S99–S107, 2000.

[57] G. P. Agrawal, *Nonlinear Fiber Optics*, 3rd ed. San Diego, CA: Academic, 2001.

[58] P. V. Mamyshev and S. V. Chernikov, "Ultrashort-pulse propagation in optical fibers," *Opt. Lett.*, vol. 15, pp. 1076–1078, 1990.

[59] J. Botineau and R. H. Stolen, "Effect of polarization on spectral broadening in optical fibers," *J. Opt. Soc. Amer.*, vol. 72, pp. 1592–1596, 1982.

[60] N. Bloembergen, *Nonlinear Optics*, 4th ed, Singapore: World Scientific, 1996.

[61] S. M. Gallagher, A. W. Albrecht, J. D. Hybl, B. L. Landin, B. Rajaram, and D. M. Jonas, "Heterodyne detection of the complete electric field of femtosecond four-wave mixing signals," *J. Opt. Soc. Amer. B*, vol. 15, pp. 2338–2345, 1998.

[62] T. Brabec and F. Krausz, "Nonlinear optical pulse propagation in the single-cycle regime," *Phys. Rev. Lett.*, vol. 78, pp. 3282–3284, 1997.

[63] S. Mukamel, *Principles of Nonlinear Optical Spectroscopy*. New York: Oxford Univ. Press, 1995.
[64] H. A. Haus and E. P. Ippen, "Group velocity of solitons," *Opt. Lett.*, vol. 26, pp. 1654–1656, 2001.
[65] X. Gu, M. W. Kimmel, E. Zeek, P. O'Shea, R. Trebino, and R. S. Windeler, "Cross-correlation frequency-resolved optical-gating measurement of ultrabroadband continuum from microstructure optical fiber," in *Ultrafast Phenomena XIII*, R. D. Miller, M. M. Murnane, N. F. Scherer, and A. M. Weiner, Eds. Berlin, Germany: Springer, 2002, pp. 193–195.
[66] M. Bellini and T. W. Hänsch, "Phase-locked white-light continuum pulses: Toward a universal optical frequency-comb synthesizer," *Opt. Lett.*, vol. 25, pp. 1049–1051, 2000.
[67] P. Baum, S. Lochbrunner, J. Piel, and E. Riedle, "Phase-coherent generation of tunable visible femtosecond pulses," *Opt. Lett.*, vol. 28, pp. 185–187, 2003.
[68] T. M. Fortier, D. J. Jones, J. Ye, and S. T. Cundiff, "Long-term carrier-envelope phase coherence," *Opt. Lett.*, vol. 27, pp. 1436–1438, 2002.
[69] T. M. Fortier, J. Ye, S. T. Cundiff, and R. S. Windeler, "Nonlinear phase noise generated in air silica microstructure fiber and its effect on carrier-envelope phase," *Opt. Lett.*, vol. 27, pp. 445–447, 2002.
[70] D. Strickland and G. Mourou, "Compression of amplified chirped optical pulses," *Opt. Commun.*, vol. 56, pp. 219–221, 1985.
[71] M. D. Perry and G. Mourou, "Terawatt to petawatt subpicosecond lasers," *Science*, vol. 264, pp. 917–924, 1994.
[72] A. Dubietis, G. Jonušaskas, and A. Piskarskas, "Powerful femtosecond pulse generation by chirped and stretched ulse parametric amplification in BBO crystal," *Opt. Commun.*, vol. 88, pp. 437–440, 1992.
[73] I. N. Ross, P. Matousek, M. Towrie, A. J. Langley, and J. L. Collier, "The prospects for ultrashort pulse duration and ultrahigh intensity using optical parametric chirped pulse amplifiers," *Opt. Commun.*, vol. 144, pp. 125–133, 1997.
[74] I. N. Ross, J. L. Collier, P. Matousek, C. N. Danson, D. Neely, R. M. Allot, D. A. Pepler, C. Hernandez-Gomez, and K. Osvay, "Generation of terawatt pulses by use of optical parametric chirped pulse amplification," *Appl. Opt.*, vol. 39, pp. 2422–2427, 2000.
[75] A. E. Siegman, *Lasers*. Mill Valley, CA: Univ. Science Books, 1986, pp. 385–386.
[76] C. Corsi and M. Bellini, "Robustness of phase coherence against amplification in a multipass femtosecond laser," *Opt. Lett.*, submitted for publication.
[77] M. S. Pshenichnikov and A. Baltuška, Unpublished, 1999.
[78] S. H. Cho, F. X. Kärtner, U. Morgner, E. P. Ippen, J. G. Fujimoto, J. E. Cunningham, and W. H. Knox, "Generation of 90-nJ pulses with a 4-MHz repetition-rate Kerr-lens mode-locked Ti:Al_2O_3 laser operating with net positive and negative intracavity dispersion," *Opt. Lett.*, vol. 26, pp. 560–562, 2001.
[79] M. S. Pshenichnikov, W. P. de Boej, and D. A. Wiersma, "Generation of 13-fs, 5-MW pulses from a cavity-dumped Ti:sapphire laser," *Opt. Lett.*, vol. 19, pp. 572–574, 1994.
[80] G. N. Gibson, R. Klank, F. Gibson, and B. E. Bouma, "Electro-optically cavity-dumped ultrashort-pulse Ti:sapphire oscillator," *Opt. Lett.*, vol. 21, pp. 1055–1057, 1996.
[81] A. Baltuška, Z. Wei, M. S. Pshenichnikov, D. A. Wiersma, and R. Szipöcs, "All-solid-state cavity-dumped sub-5-fs laser," *Appl. Phys. B*, vol. 65, pp. 175–188, 1997.
[82] F. W. Helbing, G. Steinmeyer, U. Keller, R. S. Windeler, J. Stenger, and H. R. Telle, "Carrier-envelope offset dynamics of mode-locked lasers," *Opt. Lett.*, vol. 27, pp. 194–196, 2002.
[83] A. Baltuška, A. Pug lys, M. S. Pshenichnikov, D. A. Wiersma, B. Hoenders, and H. Ferwerda, "How to retrieve amplitude and phase from autocorrelation amd spectrum," in *Tech. Dig. 2nd Int. Conf. Ultrafasts Optics '99*, Monte Verità, Ascona, Switzerland.
[84] F. Krausz, T. Brabec, M. Schnürer, and C. Spielmann, "Extreme nonlinear optics: Exposing matter to a few periods of light," *Opt. Photon. News.*, vol. 9, pp. 46–50, 1998.
[85] E. Cormier and P. Lambropoulos, "Effect of the initial phase of the field in ionization by ultrashort laser pulses," *Euro. Phys. J. D*, vol. 2, pp. 15–20, 1998.
[86] M. Kakehata, Y. Kobayashi, H. Takada, and K. Torizuka, "Single-shot measurement of a carrier-envelope phase by use of a time-dependent polarization pulse," *Opt. Lett.*, vol. 27, pp. 1247–1249, 2002.
[87] K. J. Schafer, B. Yang, L. F. DiMauro, and K. C. Kulander, "Above threshold ionization beyond the high harmonic cutoff," *Phys. Rev. Lett.*, vol. 70, pp. 1599–1602, 1993.
[88] C. Kan, N. H. Burnett, C. E. Capjack, and R. Rankin, "Coherent XUV generation from gases ionized by several cycle optical pulses," *Phys. Rev. Lett.*, vol. 79, pp. 2971–2974, 1997.
[89] N. Milosevic, A. Scrinzi, and T. Brabec, "Numerical characterization of high harmonic attosecond pulses," *Phys. Rev. Lett.*, vol. 88, pp. 093 905/1–4, 2002.
[90] V. S. Yakovlev and A. Scrinzi, "High harmonic imaging of few-cycle laser pulses," Phys. Rev. Lett., 2003, submitted for publication.
[91] E. Priori, G. Cerullo, M. Nisoli, S. Stagira, S. De Silvestri, P. Villoresi, L. Poletto, P. Ceccherini, C. Altucci, R. Bruzzese, and C. de Lisio, "Nonadiabatic three-dimensional model of high-order harmonic generation in the few-optical-cycle regime," *Phys. Rev. A*, vol. 61, pp. 063 801/1–8, 2000.
[92] M. Nisoli, G. Sansone, S. Stagira, S. De Silvestri, C. Vozzi, M. Pascolini, L. Poletto, P. Viloresi, and G. Tondello, "Effects of carrier-envelope phase differences of few-optical-cycle light pulses in single-shot high-order harmonic spectra," *Phys. Rev. Lett.*, 2003.
[93] J. Itatani, F. Quéré, G. L. Yudin, M. Y. Ivanov, F. Krausz, and P. B. Corkum, "Attosecond streak camera," *Phys. Rev. Lett.*, vol. 88, pp. 173 903/1–4, 2002.
[94] M. Kitzler, N. Milosevic, A. Scrinzi, F. Krausz, and T. Brabec, "Quantum theory of attosecond XUV pulse measurement by laser dressed photoionization," *Phys. Rev. Lett.*, vol. 88, pp. 173 904/1–4, 2002.
[95] H. Niikura, F. Légaré, R. Hasbani, A. D. Bandrauk, M. Y. Ivanov, D. M. Villeneuve, and P. B. Corkum, "Sub-laser-cycle electron pulses for probing molecular dynamics," *Nature*, vol. 417, pp. 917–922, 2002.
[96] H. Niikura, F. Legare, R. Hasbani, M. Ivanov, D. Villeneuve, and P. Corkum, "Probing molecular dynamics with attosecond resolution using correlated wave packet pairs," *Nature*, vol. 421, pp. 826–829, 2003.

Andrius Baltuška received the diploma in physics from Vilnius University, Lithuania, in 1993 and the Ph.D. degree in chemical physics from the University of Groningen, The Netherlands, in 2000. His dissertation research was conducted in the group of Prof. D. A. Wiersma and involved femtosecond nonlinear spectroscopy and generation and characterization of ultrashort laser pulses.

From 2000 to 2002, he was a Research Associate in the Ultrafast Spectroscopy Group of Prof. T. Kobayashi at the University of Tokyo, Japan. In 2002, he joined the group of Prof. F. Krausz at the Photonics Institute of Vienna University of Technology as a Post-Doctoral Fellow of the European ATTO Network. His current research interests include high-field physics and generation and applications of intense fully controlled laser pulses.

Matthias Uiberacker was born in Vienna, Austria, in 1975. He received the Diploma degree in electrical engineering from Vienna University of Technology, Austria, in 2001. He is currently working toward the Ph.D. degree at the Photonics-Institute of the Vienna University of Technology, Austria, in the group of Prof. Krausz.

His current research interests include generation, metrology, and applications of attosecond pulses.

Eleftherios Goulielmakis was born in Heraklion, Greece, on May 18, 1975. He received his B.Sc. Degree in Physics from the University of Crete in 2000 and his M.Sc. in optoelectronics from the same university in 2002. His is currently working toward his Ph.D. degree at the institute of Photonics of the Technical University of Vienna, under the supervision of Prof. F. Krausz.

His research interests include generation and applications of ultrashort laser pulses, attosecond pulse generation based on high order harmonics, and ultrafast spectroscopy.

Reinhard Kienberger was born in Graz, Austria, in 1971. He received the Diploma degree in electronics in 1999 and the Ph.D. degree in 2002, both from Vienna University of Technology, Austria.

He is currently with the Ultrafast Optics Group of Prof. F. Krausz, Vienna University of Technology, as a postdoctoral Researcher. His research interests include attosecond metrology and spectroscopy.

Vladislav S. Yakovlev received the B.Sc. degree in physics in 1997 and the M.S. degree in 1999, both from the Novosibirsk State University, Russia. He received the Ph.D. degree from Vienna University of Technology, Vienna, Austria, in 2003.

Since 2000, he has been working in the Institute of Photonics, Vienna University of Technology, involved in theoretical investigations in the field of ultrafast phenomena and design of chirped multiplayer dielectric optical coatings.

Thomas Udem was born on September 25, 1962, in Bayreuth, Germany. From 1987 to 1993, he studied physics at the University of Giessen, Germany, and at the University of Washington, Seattle. In 1993, he received the diploma from the University of Giessen, and received the Ph.D. degree from the Max-Planck-Institut für Quantenoptik, Ludwigs Maximilians Universität Munich, Germany, in 1997.

Since then, he has been working as a postdoctoral Researcher at the Max-Planck Institut für Quantenoptik and at the National Institute for Standards and Technology, Boulder, CO. His research interests include laser physics, nonlinear optics, and optical frequency measurements.

Theodor W. Hänsch received the Ph.D. degree from the Universities of Heidelberg, Germany, in 1969.

In 1970, he came to the U.S. to work as a postdoctoral Researcher with A. L. Schawlow at Stanford University, Stanford, CA. Two years later, he joined the Stanford Physics faculty as an Associate Professor. From 1975 to 1986, he was a tenured Full Professor at Stanford. In 1986, he returned to his native Germany to become Director at the Max-Planck-Institut für Quantenoptik, Garching, and Professor of Physics at the Ludwig-Maximilians-Universität, Munich. He has authored and co-authored more than 400 papers, focusing on coherent nonlinear interactions between light and matter, and holds 20 patents.

Ferenc Krausz received the diploma from Budapest University of Technology in 1985.

He is a Professor of electrical engineering at the Vienna University of Technology, Vienna, Austria, and Director at the Max-Planck-Institute for Quantum Optics (Garching, Munich, Germany). His research interests include ultrafast optics, high-field physics, and time-resolved spectroscopy.

Dr. Krausz received the Carl-Zeiss Research Award (Germany, 1998), the Wittgenstein Prize (Austria, 2002), and the Julius-Springer Prize (USA-Germany, 2003) and is a member of the Austrian Academy of Sciences.